The equity option volatility smile: an implicit finite-difference approach

Leif B. G. Andersen and Rupert Brotherton-Ratcliffe

This paper illustrates how to construct an unconditionally stable finite-difference lattice consistent with the equity option volatility smile. In particular, the paper shows how to extend the method of forward induction on Arrow–Debreu securities to generate local instantaneous volatilities in implicit and semi-implicit (Crank–Nicholson) lattices. The technique developed in the paper provides a highly accurate fit to the entire volatility smile and offers excellent convergence properties and high flexibility of asset- and time-space partitioning. Contrary to standard algorithms based on binomial trees, our approach is well suited to price options with discontinuous payouts (e.g. knock-out and barrier options) and does not suffer from problems arising from negative branching probabilities.

1. INTRODUCTION

The Black–Scholes option pricing formula (Black and Scholes 1973, Merton 1973) expresses the value of a European call option on a stock in terms of seven parameters: current time t, current stock price S_t, option maturity T, strike K, interest rate r, dividend rate γ, and volatility[1] θ. As the Black–Scholes formula is based on an assumption of stock prices following geometric Brownian motion with constant process parameters, the parameters r, γ, and θ are all considered constants independent of the particular terms of the option contract. Of the seven parameters in the Black–Scholes formula, all but the volatility θ are, in principle, directly observable in the financial market. The volatility θ can be estimated from historical data or, as is more common, by numerically inverting the Black–Scholes formula to back out the level of θ—the *implied volatility*—that is consistent with observed market prices of European options.

Although the Black–Scholes pricing formula has become the *de facto* standard in many options markets, it is generally recognized that the assumptions underlying the formula are imperfect. For example, the existence of term structures in interest rates and dividends indicate that r and γ are not constants but (at least) functions of t and T. More seriously, backing out implied volatilities from the Black–Scholes formula frequently yields θ's that are functions of maturity and stroke. Dependent on the shape of the mapping $K \mapsto \theta(S_t, t; K, T)$, the phenomenon of time- and strike-dependent volatilities is referred to as the *volatility smile* or the *volatility skew*; its existence indicates that the true probability distribution of stock prices deviates from the ideal log-normal distribution of the a Black–Scholes analysis. In the 70s and early 80s, the

volatility smile in US equity options was relatively mild and frequently either ignored by market participants or handled in an *ad hoc* manner; indeed, using S&P 500 options data from 1976 to 1978, Rubinstein (1985) detects no economic significance of the errors associated with using a constant volatility for options with the same maturity but different strikes. The crash in 1987, however, appears to have increased the likelihood assigned by the financial markets to extreme stock market movements, in particular large *downward* movements. Sometimes known as 'crash-o-phobia', this change in view of stock price dynamics has resulted in a persistent, pronounced volatility smile in current options markets (Shimko 1993, Rubinstein 1994).

Traditionally, the problems of nonconstant parameters in the models have been handled pragmatically by simply maintaining vectors and tables of r, γ, and θ to be used with different option maturities and strikes. Although this approach—by construction—works well for European options, it is unsuited for pricing of more complicated structures such as exotic options and options with early exercise features (Bermuda and American options). Consider, for example, a 2-year knock-out option with a strike of \$100 and a knock-out level of \$90. In interpolating a value of θ for the knock-out option from a (K, T) table of implied call option volatilities, should one use \$100 or \$90 (or some third value) for K? And should one use 2 years as T or, given that the option can be knocked out before it reaches its final maturity, some lower value?[2]

To answer questions like the one above, many researchers have attempted to develop models that are consistent with the existence of a volatility smile. One line of research has focused on enriching the Black–Scholes analysis by introducing additional sources of risk, including Poisson jumps (Merton 1976) and stochastic volatility (Hull and White 1987). Besides being difficult to implement and calibrate, such models lack completeness and do not allow for arbitrage-free pricing. To preserve completeness and avoid having to make assumptions about investor preferences and behavior, many newer approaches stay within the Black–Scholes one-factor diffusion framework, but introduce extra degrees of freedom by allowing the instantaneous local volatility to be a function of both time and stock levels. As it turns out, this framework is sufficiently rich to allow a perfect fit to most reasonable volatility smiles and at the same time preserves completeness and allows for application of the usual arbitrage-free pricing techniques.

The option models based on one-factor stock diffusions take several forms. In one approach, the local volatility function is prescribed directly, typically as a well-behaved function of only a few parameters (Cox and Ross 1976, Beckers 1980, Platen and Schweizer 1994). The specification of the volatility function can for example be based on a microeconomic analysis of interactions between agents in the options market, as in Platen and Schweizer (1994). Although sometimes quite realistic smiles and skews can be generated from a direct parametrization of local volatility, it is, in general, not likely that this approach will lead to a satisfactory fit to the market smile. In this paper, we instead choose to focus on an alternative, more recent, modeling technique which takes

the market volatility smile as a direct input and, through numerical or analytical techniques, backs out an implied local volatility function that is consistent with the observed volatility smile. One early effort along these lines was made by Dupire (1994), who develops a continuous-time theory in a setting without interest rates and dividends. Dupire's continuous-time results have been supplemented by a number of discrete-time numerical methods, mostly set in a binomial framework. The fit to the volatility smile is obtained through careful manipulation of the local branching probabilities in the binomial tree. Examples of such so-called *implied binomial trees* can be found in Rubinstein (1994, 1995), Derman and Kani (1994), Barle and Cakici (1995), and Chriss (1996).

The method of implied binomial trees offers a relatively straightforward approach to fitting the volatility smile, but suffers from a number of fundamental problems. First, the degrees of freedom at each tree node are not sufficiently high to guarantee that all binomial branching probabilities are nonnegative,[3] particularly in environments with high interest rates and steep volatility smiles. The heuristic rules that are typically applied to override nodes where illegal branching occurs (see Derman and Kani 1994) are not only unsatisfactory but result in loss of local process information that can easily compound up to significant pricing errors (Barle and Cakici 1995). A second problem of binomial trees has been documented by Boyle and Lau (1994), who illustrate how using binomial trees to price options with discontinuous payouts (such as barrier and knock-out options) can lead to extremely erratic convergence behavior unless care is taken to align the asset partitioning of the tree with the option barrier. As binomial trees have very limited flexibility in setting the partitioning of the asset space—in fact, the asset grid can essentially only be affected indirectly through the choice of number of time-steps—this alignment process can frequently put severe constraints on the overall design of the lattice. For implied binomial trees, the alignment process is generally not even possible, as the time- and asset-varying nature of the branching process results in trees where the asset-partitioning of each time slice is unique and not aligned with the asset levels of other slices.

Whereas the implied binomial tree is primarily based on a discretization of the stock price process, this paper will focus on developing a discrete-time model by discretizing the fundamental no-arbitrage partial differential equation (PDE). This discretization is accomplished by an adaptation of the method of *finite differences* (see, for example, Brennan and Schwartz 1978, Courtadon 1982, Geske and Shastri 1985, Hull and White 1990, and Dewynne *et al.* 1993). The application of one particularly simple finite-difference scheme, the so-called *explicit scheme* (or *trinomial tree*), to the volatility smile problem has been described by Dupire (1994) and, in a purely probabilistic setting, by Derman *et al.* (1996). As we will show in the paper, the explicit finite-difference method, however, suffers from many of the same problems as the binomial tree and is prone to instability. In this paper, we instead focus on an alternative class of algorithms known as implicit and semi-implicit (Crank–Nicholson) finite-difference schemes. While somewhat more complicated to evaluate and calibrate, the implicit and semi-implicit schemes

are shown to exhibit much better stability and convergence properties than trinomial and binomial trees. Further, contrary to the binomial algorithm, the algorithms developed in this paper do not involve explicit adjustments of branching probabilities and allow for completely independent prescription of the stock- and time-partitionings. The high partitioning flexibility permits control of convergence behavior as it allows for perfect alignment of time- and asset-slices with important dates (e.g. dividends, average sampling dates, trigger observation dates, etc.) and price levels (e.g. strikes, barriers, etc.).

While our numerical approach is different, our paper is similar in spirit to the original work by Dupire (1994). In particular, we assume the existence of a complete, spanning set of European call option prices, which, in practice, requires usage of extrapolation and interpolation methods. An alternative approach (e.g. Avallaneda *et al.* 1996, Lagnado and Osher 1997, and Brown and Toft 1996) is to work only with actively traded options and 'fill in' the gaps indirectly through assumptions about market behavior and regularity. While this approach has its merits, it yields less control over the resulting volatility surfaces and, as large-scale nonlinear optimization is typically necessary, is much slower than the method used in this paper.

The rest of this paper is organized as follows. In Section 2, we summarize the continuous-time theory of Dupire (1994) and provide some extensions to include nonzero dividends and interest rates. Section 3, the main section of the paper, develops the theory of our implicit finite-difference approach. In Section 4, we test the accuracy and convergence properties of the finite-difference algorithm and exemplify its application to exotic options by pricing down-and-out knock-out call options. Finally, Section 5 summarizes the results of the paper and briefly discusses extensions and generalizations.

2. CONTINUOUS TIME

In this section, we present the continuous-time theory behind the one-factor diffusion approach to modeling the dynamics of the volatility smile. The material in this section is based on Dupire (1994), but is set in a more general framework.

Let us consider a frictionless economy in which a traded asset S is driven by a one-factor diffusion process of the form

$$\mathrm{d}S_t/S_t = \mu(S_t, t)\,\mathrm{d}t + \sigma(S_t, t)\,\mathrm{d}W_t, \qquad S_0 = S_{\mathrm{ini}} > 0, \quad t \in [0, \tau]. \tag{1}$$

for some fixed trading horizon τ and some positive constant time 0 value S_{ini}. In (1), W_t is a Brownian motion with respect to the real-world probability measure and $\mu,\sigma : \mathbb{R}^+ \times [0,\tau] \to \mathbb{R}$ are deterministic functions sufficiently well behaved to ensure that (1) has a unique solution (see Arnold 1974: Chap. 6). We will assume that S pays dividends at a time-varying, but deterministic, rate of $\gamma(t)$. For fixed $t \in [0,\tau]$ and all

$T \in [t, \tau]$ we further assume the existence of zero-coupon bonds $P(t, T)$; the evolution of the zero-coupon bond term structure is assumed to be deterministic, i.e.

$$P(T_1, T_2) = P(t, T_2)/P(t, T_1), \qquad 0 \leqslant t \leqslant T_1 \leqslant T_2 \leqslant \tau. \tag{2}$$

The instantaneous interest rate r is a deterministic function of time given by

$$P(t, T) = \exp[-\int_t^T r(u)\,\mathrm{d}u] \quad \Rightarrow \quad r(t) = \frac{\partial P(t, T)/\partial t}{P(t, T)} = \frac{\partial\big(P(0, T)/P(0, t)\big)}{\partial t}\frac{P(0, t)}{P(0, T)}$$
$$= \frac{-\partial P(0, t)/\partial t}{P(0, t)}, \quad 0 \leqslant t \leqslant T \leqslant \tau. \tag{3}$$

We now introduce a contingent claim on the asset S with final maturity $T \in [0, \tau]$ and payout function $g : \mathbb{R}^+ \to \mathbb{R}$. Arbitrage arguments (see Merton 1973) show that the value of the contingent claim at any time before T equals $V(S_t, t)$ where $V : \mathbb{R}^+ \times [0, \tau] \to \mathbb{R}$ satisfies the *no-arbitrage PDE*

$$\frac{\partial V(S, t)}{\partial t} + \tfrac{1}{2}\sigma^2(S, t)S^2\frac{\partial^2 V(S, t)}{\partial S^2} + [r(t) - \gamma(t)]S\frac{\partial V(S, t)}{\partial S} = r(t)V(S, t), \qquad t \in [0, T) \tag{4}$$

with boundary condition

$$V(S_T, T) = g(S_T). \tag{5}$$

Under regularity conditions on r, γ, and σ, the Feynman–Kac theorem (see Karatzas and Shreve 1991) shows that the solution to (4) can be written as an expectation

$$V(S, t) = P(t, T)\int_0^\infty g(u)p(S, t; u, T)\,\mathrm{d}u, \qquad 0 \leqslant t \leqslant T, \tag{6}$$

where $p(\,\cdot\,)$ is the *risk-neutral transition density function* of S (also known as the *Green's function* or the *fundamental PDE solution*). $p(\,\cdot\,)$ satisfies the Kolmogorov forward (or Fokker–Planck) equation (see e.g. Cox and Miller 1965: Chap. 5)

$$\frac{\partial p}{\partial T} + \frac{\partial([r(T) - \gamma(T)]up)}{\partial u} - \tfrac{1}{2}\frac{\partial^2\big(\sigma^2(u, T)u^2p\big)}{\partial u^2} = 0 \quad \text{for fixed } (S, t), T \in (t, \tau]. \tag{7}$$

The boundary condition to (7) is $p(S, t; u, t) = \delta(S - u)$, where $\delta(\,\cdot\,)$ is the *Dirac delta-function*.

In this paper, we will pay particular attention to *European call options* $C(S_t, t)$ with payout function

$$g(S_T) = C(S_T, T) = \max(S_T - K, 0), \qquad K > 0. \tag{8}$$

In the special case of a constant volatility, $\sigma(S_t, t) = \theta > 0$, the solution to (4) subject to (8) can be written in closed form as the (extended) *Black–Scholes formula*:

$$C_{\mathrm{BS}}(S_t, t; T, K, \theta) = S_t \exp\Big[-\int_t^T \gamma(u)\,\mathrm{d}u\Big]N(d_+) - P(t, T)KN(d_-), \qquad t \in [0, T), \tag{9}$$

$$d_{\pm} = \frac{\ln(S_t/K) + \int_t^T [r(u) - \gamma(u)]\,\mathrm{d}u}{\theta\sqrt{T-t}} \pm \tfrac{1}{2}\theta\sqrt{T-t},$$

where $N(\,\cdot\,)$ is the standard cumulative normal distribution function.

Returning to the general case of nonconstant volatility, observe that, for the European call, (6) is particularly simple:

$$C(S,t;K,T) = P(t,T)\int_K^\infty (u-K)p(S,t;u,T)\,\mathrm{d}u. \tag{10}$$

Using Leibniz's rule to differentiate (10) twice with respect to K yields

$$p(S,t;K,T) = \frac{1}{P(t,T)}\frac{\partial^2 C(S,t;K,T)}{\partial^2 K}. \tag{11}$$

Given a continuum of traded European calls with different strikes and maturities, (11) shows that the risk-neutral transition densities of S can be recovered directly from market prices, an observation originally due to Breeden and Litzenberger (1978).

Using (11), the first term in the forward equation (7) becomes

$$\frac{\partial p}{\partial T} = \frac{1}{P(t,T)}\frac{\partial\left(\partial^2 C/\partial K^2\right)}{\partial T} + \frac{\partial^2 C}{\partial K^2}\frac{\partial\left(1/P(t,T)\right)}{\partial T} = \frac{1}{P(t,T)}\left(\frac{\partial^2}{\partial K^2}\frac{\partial C}{\partial T} + \frac{\partial^2 C}{\partial K^2}r(T)\right). \tag{12}$$

Applying (11) to the remaining terms in (7) gives

$$\frac{\partial^2}{\partial K^2}\frac{\partial C}{\partial T} + \frac{\partial^2 C}{\partial K^2}r(T) + [r(T)-\gamma(T)]\frac{\partial\left(K(\partial^2 C/\partial K^2)\right)}{\partial K} = \tfrac{1}{2}\frac{\partial^2\left(\sigma^2(K,T)K^2(\partial^2 C/\partial K^2)\right)}{\partial K^2}, \tag{13}$$

which can be integrated twice with respect to K to yield

$$\frac{\partial C}{\partial T} + r(T)C + [r(T)-\gamma(T)]\left(K\frac{\partial C}{\partial K} - C\right) = \tfrac{1}{2}\sigma^2(K,T)K^2\frac{\partial^2 C}{\partial K^2} + A(T)K + B(T), \tag{14}$$

where A and B are arbitrary functions of time. Following Dupire (1994), we assume that the functions involved in (14) have sufficient regularity to make all terms involving C approach zero as K approaches infinity. Under this assumption, the integration functions A and B must be zero. The forward PDE (14) is strikingly similar to the general pricing (backward) PDE (4), but whereas (4) holds for arbitrary option payouts, (14) is only valid for European calls (and puts). From (14) we obtain the following result.

Proposition 1. Let S follow a continuous-time one-factor diffusion of the form (1) and let there be given observable arbitrage-free market prices of European calls for all strikes $K \in [0,\infty)$ and all maturities $T \in (t,\tau]$. The instantaneous volatility function of S that is consistent with the market is given uniquely by

$$\sigma^2(K,T) = 2\,\frac{\partial C/\partial T + \gamma(T)C + K[r(T)-\gamma(T)]\partial C/\partial K}{K^2(\partial^2 C/\partial K^2)}, \tag{15}$$

or, written in terms of the observed implied volatility smile[4] $\theta(S_t, t; K, T)$,

$$\sigma^2(K,T) = \frac{2\dfrac{\partial\theta}{\partial T} + \dfrac{\theta}{T-t} + 2K[r(T)-\gamma(T)]\dfrac{\partial\theta}{\partial K}}{K^2\left[\dfrac{\partial^2\theta}{\partial K^2} - d_+\sqrt{T-t}\left(\dfrac{\partial\theta}{\partial K}\right)^2 + \dfrac{1}{\theta}\left(\dfrac{1}{K\sqrt{T-t}} + d_+\dfrac{\partial\theta}{\partial K}\right)^2\right]}, \tag{16}$$

where d_+ is defined in (9).

Proof. Equation (15) follows immediately from (14), and (16) follows, after some manipulations, from (15) and (9). To verify that $\sigma(K,T)$ is a real number, i.e. that $\sigma^2(K,T) \geqslant 0$, we notice from (11) that it suffices to show that the numerator in (15) is nonnegative in the absence of arbitrage. Portfolio dominance arguments similar to those in Merton (1973) imply the following result:

$$\mathrm{e}^{\int_T^{T_1}\gamma(u)\,\mathrm{d}u} C\left(S_t, t; K\,\mathrm{e}^{\int_T^{T_1}[r(u)-\gamma(u)]\,du}, T_1\right) \geqslant C(S_t, t; K, T), \qquad T_1 > T.$$

Setting $T_1 = T + \varepsilon$ in the left-hand side of the above inequality and evaluating the limit as $\varepsilon \to 0_+$ yields

$$\frac{\partial C}{\partial T} + \gamma(T)C + K([r(T)-\gamma(T)]\frac{\partial C}{\partial K} \geqslant 0. \qquad \square$$

For the special case of strike-independent implied volatility, (16) reduces to the well-known expression

$$\sigma^2(T) = \theta^2(T) + 2(T-t)\theta(T)\frac{\partial\theta}{\partial T},$$

or

$$\frac{1}{T-t}\int_t^T \sigma^2(s)\,\mathrm{d}s = \theta^2(T).$$

3. DISCRETE TIME

While equations (15) and (16) in combination with the no-arbitrage PDE (4) exhaust the theoretical specification of the volatility smile model, in practice numerical methods must be introduced to calculate the prices of specific contingent claims. As discussed in Section 1, most such schemes suggested in the current literature are based on a binomial approximation of the stochastic differential equation (1). In this section, we will develop an alternative to the binomial method using the method of finite differences.

3.1 Discretization Scheme

To increase the efficiency of the finite-difference discretization, we first shift variables in the PDE (4). Specifically, we put $x = \ln S$ and $H(x,t) = V(S,t)$ so that the governing

equation becomes

$$\frac{\partial H(x,t)}{\partial t} + \tfrac{1}{2} v(x,t) \frac{\partial^2 H(x,t)}{\partial x^2} + b(x,t) \frac{\partial H(x,t)}{\partial x} = r(t) H(x,t), \tag{17}$$

where

$$b(x,t) = r(t) - \gamma(t) - \tfrac{1}{2} v(x,t), \qquad v(x,t) = \sigma^2(S,t) = \sigma^2(\mathrm{e}^x, t).$$

At this point, we could use the continuous-time dividend term structure $\gamma(t)$, the interest rate term structure (3) and the instantaneous volatility equations (15) and (16) to discretize (17) directly. However, as the coefficients in (17) would then all be based on results from a continuous-time setting, such a discretization would only in the limit yield correct prices of traded bonds and stock derivatives. To improve convergence and accuracy of discrete-time prices, we replace the continuous-time coefficients in (17) by unknown functions $\hat{r}(t)$, $\hat{b}(x,t)$, and $\hat{v}(x,t)$ which shall be solved for so that our discretization of the backward PDE will return the correct market prices of stock forwards, zero-coupon bonds, and European options. We point out that $\hat{r}(t)$, $\hat{b}(x,t)$, and $\hat{v}(x,t)$ will depend on both the discretization scheme and the selected spacing between grid points.

Now consider determining the time-0 value of a contingent claim with final maturity $0 < T < \tau$. To discretize (17), we divide the (x,t) plane into a uniformly spaced mesh with $M+2$ nodes along the t axis and $N+2$ nodes along the x axis:

$$x_i = x_0 + i\Delta_x = x_0 + i\frac{x_{N+1} - x_0}{N+1}, \qquad i = 0, \ldots, N+1, \tag{18a}$$

$$t_j = j\Delta_t = j\frac{T}{M+1}, \qquad j = 0, \ldots, M+1. \tag{18b}$$

The indices $i = 0$, $i = N+1$, $j = 0$, $j = M+1$ signify the limits of the mesh for which boundary conditions must be prescribed. The values of x_0 and x_{N+1} should be set sufficiently low and high, respectively, to ensure that most of the statistically significant x space is captured by the mesh.[5] Without loss of generality, we assume that the time-0 stock value S_{ini} is contained in the mesh,[6] i.e.

$$x_{\text{ini}} \equiv \ln S_{\text{ini}} = x_\beta, \tag{19}$$

for some integer $\beta \in [1, N]$. We point out that the finite-difference method does not rely on an equidistant partitioning of t and x space (as in (18a,b)); for the sake of simplicity, however, we maintain the assumption of a uniform mesh throughout this paper.

At an arbitrary node (x_i, t_j), with $i = 1, \ldots, N$, $j = 0, \ldots, M$ in the grid (18a,b) we introduce the following difference approximations to the terms in the PDE (17):

$$\frac{\partial H}{\partial t} \approx \frac{H(x_i, t_{j+1}) - H(x_i, t_j)}{\Delta_t}, \tag{20a}$$

$$\frac{\partial H}{\partial x} \approx (1-\Theta)\frac{H(x_{i+1}, t_j) - H(x_{i-1}, t_j)}{2\Delta_x} + \Theta\frac{H(x_{i+1}, t_{j+1}) - H(x_{i-1}, t_{j+1})}{2\Delta_x}, \tag{20b}$$

$$\frac{\partial^2 H}{\partial x^2} \approx (1-\Theta)\frac{H(x_{i+1},t_j)-2H(x_i,t_j)+H(x_{i-1},t_j)}{\Delta_x^2} + \Theta\frac{H(x_{i+1},t_{j+1})-2H(x_i,t_{j+1})+H(x_{i-1},t_{j+1})}{\Delta_x^2}. \quad (20c)$$

The parameter $\Theta \in [0,1]$ determines the time at which partial derivatives w.r.t. x are evaluated. If $\Theta = 0$, the x derivatives are evaluated at time t_j and the differencing scheme gives rise to the *fully implicit finite-difference method*. If $\Theta = 1$, the x derivatives are evaluated one time-step ahead, at t_{j+1}, and the resulting scheme is known as the *explicit finite-difference method*. Finally, when $\Theta = \frac{1}{2}$, the x derivatives are evaluated half a time-step ahead, at $\frac{1}{2}(t_j + t_{j+1})$; the resulting scheme is an average of the explicit and implicit schemes known as the *Crank–Nicholson* scheme. Values of Θ different from 0, $\frac{1}{2}$, and 1 are possible but little used in practice.

Plugging (20a–c) into (17) and substituting $\hat{b}$, $\hat{r}$, $\hat{v}$ for b, r, and v, respectively, yields the recursive relation for $i = 1,\ldots,N$ and $j = 0,\ldots,M$ (with $H_{i,j} \equiv H(x_i,t_j)$, etc.):

$$\begin{aligned} &H_{i-1,j}\left(-\tfrac{1}{2}\alpha(1-\Theta)(\hat{v}_{i,j}-\Delta_x\hat{b}_{i,j})\right) \\ &\quad +H_{i,j}\left(1+\hat{r}_j\Delta_t+\alpha(1-\Theta)\hat{v}_{i,j}\right)+H_{i+1,j}\left(-\tfrac{1}{2}\alpha(1-\Theta)(\hat{v}_{i,j}+\Delta_x\hat{b}_{i,j})\right) \\ &= H_{i-1,j+1}\left(\tfrac{1}{2}\alpha\Theta(\hat{v}_{i,j}-\Delta_x\hat{b}_{i,j})\right)+H_{i,j+1}(1-\alpha\Theta\hat{v}_{i,j})+H_{i+1,j+1}\left(\tfrac{1}{2}\alpha\Theta(\hat{v}_{i,j}+\Delta_x\hat{b}_{i,j})\right), \quad (21) \end{aligned}$$

where $\alpha \equiv \Delta_t/\Delta_x^2$.

Equation (21) can be written compactly in matrix notation as

$$[(1+\hat{r}_j\Delta_t)\boldsymbol{I}-(1-\Theta)\boldsymbol{M}_j]\boldsymbol{H}_j = \left(\Theta\boldsymbol{M}_j+\boldsymbol{I}\right)\boldsymbol{H}_{j+1}+\boldsymbol{B}_j, \qquad j=0,\ldots,M, \quad (22)$$

where $\boldsymbol{I}$ is the $N \times N$ identity matrix, $\boldsymbol{H}_j$ and $\boldsymbol{H}_{j+1}$ are $N \times 1$ vector of contingent claim values,

$$\boldsymbol{H}_j \equiv \begin{bmatrix} H_{1,j} \\ H_{2,j} \\ \vdots \\ H_{N,j} \end{bmatrix},$$

$\boldsymbol{B}_j$ is a $N \times 1$ vector that contains the prescribed values of H along the x boundary of the mesh,

$$\boldsymbol{B}_j \equiv \begin{bmatrix} l_{1,j}[(1-\Theta)H_{0,j}+\Theta H_{0,j+1}] \\ 0 \\ 0 \\ \vdots \\ 0 \\ u_{N,j}[(1-\Theta)H_{N+1,j}+\Theta H_{N+1,j+1}] \end{bmatrix},$$

and $\boldsymbol{M}_j$ is a tridiagonal $N \times N$ matrix

$$\boldsymbol{M}_j \equiv \begin{bmatrix} c_{1,j} & u_{1,j} & 0 & 0 & 0 & \cdots & 0 \\ l_{2,j} & c_{2,j} & u_{2,j} & 0 & 0 & \cdots & 0 \\ \vdots & \vdots & \vdots & \vdots & \vdots & \vdots & \vdots \\ 0 & 0 & 0 & \cdots & l_{N-1,j} & c_{N-1,j} & u_{N-1,j} \\ 0 & 0 & 0 & \cdots & 0 & l_{N,j} & c_{N,j} \end{bmatrix},$$

where

$$c_{i,j} = -\alpha \hat{v}_{i,j}, \tag{23a}$$

$$u_{i,j} = \tfrac{1}{2}\alpha(\hat{v}_{i,j} + \Delta_x \hat{b}_{i,j}), \tag{23b}$$

$$l_{i,j} = \tfrac{1}{2}\alpha(\hat{v}_{i,j} - \Delta_x \hat{b}_{i,j}). \tag{23c}$$

If the matrices in (22) can be determined, i.e. if the values of $\hat{r}_j$, $\hat{b}_{i,j}$, and $\hat{v}_{i,j}$ are known, the price of a contingent claim at time 0 can be obtained by iteratively solving the system of linear equations (22) backwards from the known time T payout vector $\boldsymbol{H}_{N+1}$. As the vector multiplying $\boldsymbol{H}_j$ is tridiagonal, the numerical solution to (22) can be coded very efficiently ($O(N)$); see e.g. Press *et al.* (1992: Chap. 2) for a discussion and specific algorithms. In Appendix A, we derive sufficient conditions for (22) to have a unique solution; these conditions will be satisfied by most realistic finite-difference meshes.

Contrary to a binomial tree where the value of a contingent claim on any given node can be determined from the state of only two nodes one time-step ahead (the 'up' and the 'down' nodes), the system of equations (22) generally links the value of $H_{i,j}$ to *all* interior values of H at time t_{j+1}, i.e. $H_{i,j} = F(H_{1,j+1}, \ldots, H_{N,j+1})$ for some function F. An exception occurs for the *explicit finite-difference scheme* ($\Theta = 1$) where the matrix multiplying $\boldsymbol{H}_j$ on the left-hand side of (22) is diagonal and $H_{i,j}$ consequently a function of only $H_{i+1,j+1}$, $H_{i,j+1}$, and $H_{i-1,j+1}$. According to (21), the equations for the explicit finite-difference scheme are

$$H_{i,j} = \frac{1}{1 + \hat{r}_j \Delta_t}\left[l_{i,j} H_{i-1,j+1} + H_{i,j+1}(1 + c_{i,j}) + u_{i,j} H_{i+1,j+1}\right]. \tag{24}$$

From (23a–c) we see that $l_{i,j} + (1 + c_{i,j}) + u_{i,j} = 1$, which allows for an interpretation of (24) as a trinomial tree with pseudo-probabilities of up, down, and center moves equal to $u_{i,j}$, $l_{i,j}$, and $1 - l_{i,j} - u_{i,j}$, respectively. While the explicit finite-difference grid has an attractive probabilistic interpretation and a simple causal structure, it unfortunately suffers from stability problems. In Appendix B, we derive conditions for the explicit finite-difference scheme to be stable; in most cases, these conditions are equivalent to all of the 'probabilities' $u_{i,j}$, $l_{i,j}$, or $1 + c_{i,j}$ being nonnegative. Due to the time-varying nature of $\hat{b}$ and $\hat{v}$, maintaining nonnegative probabilities at all nodes in the mesh puts heavy constraints on the spacing of the finite-difference mesh and, as in the binomial setting, turns out to interfere quite significantly with the fitting of the volatility smile. Consequently, the rest of this paper will *assume that* $\Theta \neq 1$ and instead focus on the Crank–Nicholson and implicit schemes which are known to have much better stability properties than the explicit scheme. Indeed, as a local harmonic analysis in Appendix B

shows, both these schemes are unconditionally stable as long as $\hat{v}_{i,j} \geqslant 0$ for all i and j in the mesh. In most cases, we recommend the Crank–Nicholson scheme which has the best convergence properties of the three schemes. Specifically, the convergence order of the Crank–Nicholson scheme[7] is $O(\Delta_t^2)$, whereas both the explicit and the implicit schemes converge as $O(\Delta_t)$. All schemes converge as $O(\Delta_x^2)$ in x space.

3.2 Fitting of Bond Prices

As in the continuous-time case, we will assume the existence of a complete initial yield curve as given by prices of traded zero-coupon bonds maturing at all mesh times, $P_j = P(0, t_j)$, $j = 1, \ldots, N+1$. As the strip of zero-coupon bonds can be interpreted as contingent claims with payout functions $g(S_{t_j}) = \$1$, their prices must satisfy the finite-difference equation (21). At time-step t_j consider the bond maturing one time-step ahead, $P(t_j, t_{j+1})$. Since, in our setting, bond prices are deterministic and thus independent of S (and x), (21) simplifies to

$$P(t_j, t_{j+1})\big(1 + \hat{r}_j \Delta_t\big) = P(t_{j+1}, t_{j+1}) = \$1, \qquad j = 1, \ldots, N. \tag{25}$$

From (2) we know that

$$\frac{1}{P(t_j, t_{j+1})} = \frac{P(0, t_j)}{P(0, t_{j+1})} = \frac{P_j}{P_{j+1}},$$

so (with $P_0 = 1$)

$$\hat{r}_j = \frac{1}{\Delta_t}\left(\frac{P_j}{P_{j+1}} - 1\right), \qquad j = 0, \ldots, N. \tag{26}$$

Not surprisingly, equation (26) is related to the continuous-time equation (3) through the finite-difference relation $\partial P(0, t_j)/\partial t \approx [P(0, t_{j+1}) - P(0, t_j)]/\Delta_t$.

3.3 Fitting of Asset Forwards

To match the drift of S, consider at time t_j a contract that pays out[8] $g(S_{t_{j+1}}) = S_{t_{j+1}}$ at the time-step t_{j+1} of the lattice. At node (x_i, t_j), the value of this contract is

$$H_{i,j} = S_i \exp\left(-\int_{t_j}^{t_{j+1}} \gamma(u)\, \mathrm{d}u\right) = \mathrm{e}^{x_i}\frac{\Gamma_{j+1}}{\Gamma_j}, \qquad i = 1, \ldots, N, \quad j = 0, \ldots, M, \tag{27}$$

where we have defined

$$\Gamma_j \equiv \exp\left(-\int_0^{t_j} \gamma(u)\, \mathrm{d}u\right).$$

Setting $H_{i,j} = S_i \Gamma_{j+1}/\Gamma_j$ and $H_{i,j+1} = S_i$ in the discretized PDE (21) and rearranging yields

$$S_i\left[1 - \frac{\Gamma_{j+1}}{\Gamma_j}(1 + \hat{r}_j \Delta_t) - \alpha \hat{v}_{i,j}\left((1-\Theta)\frac{\Gamma_{j+1}}{\Gamma_j} + \Theta\right)\right] + (S_{i+1} + S_{i-1})\left[\tfrac{1}{2}\alpha \hat{v}_{i,j}\left((1-\Theta)\frac{\Gamma_{j+1}}{\Gamma_j} + \Theta\right)\right]$$
$$+ (S_{i+1} - S_{i-1})\left[\tfrac{1}{2}\alpha \Delta_x \hat{b}_{i,j}\left((1-\Theta)\frac{\Gamma_{j+1}}{\Gamma_j} + \Theta\right)\right] = 0, \qquad i = 1, \ldots, N, \quad j = 0, \ldots, M. \tag{28}$$

Now

$$S_{i+1} + S_{i-1} = S_i e^{\Delta_x} + S_i e^{-\Delta_x} = 2S_i \cosh \Delta_x, \qquad S_{i+1} - S_{i-1} = S_i e^{\Delta_x} - S_i e^{-\Delta_x} = 2S_i \sinh \Delta_x$$

so (28) becomes

$$\frac{1 - (\Gamma_{j+1}/\Gamma_j)(1 + \hat{r}_j \Delta_t)}{(1 - \Theta)(\Gamma_{j+1}/\Gamma_j) + \Theta} + \alpha \hat{v}_{i,j}(\cosh \Delta_x - 1) + \alpha \hat{b}_{i,j} \Delta_x \sinh \Delta_x = 0. \tag{29}$$

Using the identity

$$\tanh \tfrac{1}{2}\Delta_x = \frac{\cosh \Delta_x - 1}{\sinh \Delta_x},$$

(29) can finally be rearranged as

$$\hat{b}_{i,j} = \frac{\Delta_x}{\Delta_t \sinh \Delta_x}\left(\frac{P_j/P_{j+1} - \Gamma_j/\Gamma_{j+1}}{(1 - \Theta) + \Theta\Gamma_j/\Gamma_{j+1}}\right) - \frac{\hat{v}_{i,j}}{\Delta_x}\tanh\frac{\Delta_x}{2}, \qquad i = 1, \ldots, N, \quad j = 0, \ldots, M, \tag{30}$$

where we have used the result (26) to eliminate $\hat{r}_j$. It can easily be verified that $\hat{b}_{i,j} \to r_j - \gamma_j - \frac{1}{2}\hat{v}_{i,j}$ when Δ_x and Δ_t approach zero.

3.3 Fitting European Call Options

Equipped with (26) and (30), the discretization (21) will yield the correct forward stock and zero-coupon bond prices, irrespective of the volatility function $\hat{v}_{i,k}$. To determine the correct local volatilities, we assume the existence of observable call option prices with strikes and maturities spanning all nodes inside the upper and lower x boundaries of the finite-difference mesh (18a,b). Let $C_{\text{ini}}^{i,j}$ denote the time-0 observable value of a European call with strike $K = S_i = e^{x_i}$ and maturity of t_j, where $i = 1, \ldots, N$ and $j = 1, \ldots, M + 1$.

While it would conceivably be possible to use brute-force trial-and-error techniques to back out a volatility function that correctly prices all calls $C_{\text{ini}}^{i,j}$ in the finite-difference mesh, this approach requires too much computational effort to be useful in practice. A significantly more efficient alternative is the so-called method of *forward induction* (Jamshidian 1991, Hull and White 1994), which avoids brute-force search by, in effect, introducing discrete-time versions of the Fokker–Planck forward equation (7) (or (14)). Rather than discretizing (7) or (14) directly, we will here use fundamental arguments to derive a discrete-time forward equation consistent with our backward discretization scheme (22). For this purpose, it is convenient and instructive to introduce the concept of *Arrow–Debreu securities*. To be specific, let $A_{\text{ini}}^{i,j}$ denote the time-0 price of a Arrow–Debreu security that at time t_j pays out \$1 if the asset price equals S_i and \$0 otherwise. To ensure correct pricing of bonds and stock forwards, the Arrow–Debreu securities must satisfy the following obvious constraints:

$$\sum_{i=0}^{N+1} A_{\text{ini}}^{i,j} = P_j, \qquad j = 0, \ldots, M + 1, \tag{31a}$$

$$\sum_{i=0}^{N+1} A_{\text{ini}}^{i,j} S_i = S_{\text{ini}}\Gamma_j, \qquad j = 0, \ldots, M + 1. \tag{31b}$$

It also follows from the definition of the European call payout function (8) that

$$C_{\text{ini}}^{i,j} = \sum_{l=i+1}^{N+1} A_{\text{ini}}^{l,j}(S_l - S_i), \qquad i = 1, \ldots, N, \quad j = 0, \ldots, M+1. \tag{32a}$$

The values of calls struck on the upper and lower x boundary cannot be specified freely[9] but are determined directly by (31a, b):

$$C_{\text{ini}}^{N+1,j} = 0, \qquad j = 0, \ldots, M+1, \tag{32b}$$

$$C_{\text{ini}}^{0,j} = \sum_{l=0}^{N+1} A_{\text{ini}}^{l,j} S_l - S_0 \sum_{l=0}^{N+1} A_{\text{ini}}^{l,j} = S_{\text{ini}}\Gamma_j - S_0 P_j, \qquad j = 0, \ldots, M+1. \tag{32c}$$

After a little algebra, (32a) can be inverted to yield Arrow–Debreu prices as a function of call prices:

$$A_{\text{ini}}^{i,j} = \frac{(S_i - S_{i-1})C_{\text{ini}}^{i+1,j} - (S_{i+1} - S_{i-1})C_{\text{ini}}^{i,j} + (S_{i+1} - S_i)C_{\text{ini}}^{i-1,j}}{(S_{i+1} - S_i)(S_i - S_{i-1})}$$

$$= \frac{\mathrm{e}^{-\frac{1}{2}\Delta_x} C_{\text{ini}}^{i+1,j} - 2\cosh\tfrac{1}{2}\Delta_x C_{\text{ini}}^{i,j} + \mathrm{e}^{\frac{1}{2}\Delta_x} C_{\text{ini}}^{i-1,j}}{2\mathrm{e}^{x_i}\sinh\tfrac{1}{2}\Delta_x}, \quad i = 1, \ldots, N, \ j = 1, \ldots, M+1. \tag{33a}$$

The Arrow–Debreu price of the upper boundary, $A_{\text{ini}}^{N+1,j}$, follows from $C_{\text{ini}}^{N,j} = A_{\text{ini}}^{N+1}(S_{N+1} - S_N)$ or

$$A_{\text{ini}}^{N+1,j} = \frac{C_{\text{ini}}^{N,j}}{S_{N+1} - S_N} = \frac{C_{\text{ini}}^{N,j}}{(\mathrm{e}^{\Delta_x} - 1)\mathrm{e}^{x_N}}, \qquad j = 1, \ldots, M+1. \tag{33b}$$

The Arrow–Debreu price of the lower boundary is given by the constraint (31a):

$$A_{\text{ini}}^{0,j} = P_j - \sum_{i=1}^{N+1} A_{\text{ini}}^{i,j} = P_j - \frac{C_{\text{ini}}^{0,j} - C_{\text{ini}}^{1,j}}{S_1 - S_0} = \frac{P_j S_1 - \Gamma_j S_{\text{ini}} + C_{\text{ini}}^{1,j}}{S_1 - S_0}$$

$$= \frac{P_j e^{\Delta_x} - \Gamma_j \mathrm{e}^{\beta\Delta_x} + C_{\text{ini}}^{1,j}/\mathrm{e}^{x_0}}{\mathrm{e}^{\Delta_x} - 1}, \qquad j = 1, \ldots, M+1, \tag{33c}$$

where the second equality follows from (32a) and the third equality from (32c). The integer β in (33c) is defined in equation (19).

The boundary condition at time 0 for the Arrow–Debreu prices is obviously

$$A_{\text{ini}}^{i,0} = \left\{ \begin{array}{ll} \$1, & \text{if } i = \beta \\ \$0, & \text{otherwise} \end{array} \right\}, \qquad i = 0, \ldots, N+1. \tag{33d}$$

Equation (33a) is the discrete-time version of the continuous-time equation (11) and illustrates the close link between Arrow–Debreu prices and the continuous-time risk-neutral density function. In particular, if we approximate the second derivative in (11) with a central finite difference, (33a) implies the relation

$$\frac{A_{\text{ini}}^{i,j}}{P_j} \approx \tfrac{1}{2}(S_{i+1} - S_{i-1})p(S_{\text{ini}}, 0; S_i, t_j). \tag{34}$$

For obvious reasons, the term $A^{i,j}_{\text{ini}}/P_j$ is sometimes known as the *Arrow–Debreu (pseudo-)probability* of node (x_i, t_j).

Being contingent claims on S, the Arrow–Debreu securities must satisfy the finite-difference equation (22). If we use the notation $A^{k,l}_{i,j}$ $(l \geqslant j)$ to denote the price at node (x_i, t_j) of the Arrow–Debreu security that pays out if and only if node (x_k, t_l) is reached (so that, in particular, $A^{k,l}_{\text{ini}} = A^{k,l}_{\beta,0}$), (22) becomes (using (26)) for a fixed interior value of k and $l = j+1$:

$$\left(\frac{P_j}{P_{j+1}}\boldsymbol{I} - (1-\Theta)\boldsymbol{M}_j\right)\boldsymbol{A}^{k,j+1}_j = \big(\Theta\boldsymbol{M}_j + \boldsymbol{I}\big)\boldsymbol{A}^{k,j+1}_{j+1} + \boldsymbol{B}^k_j, \qquad j = 0,\ldots,M, \quad k = 1,\ldots,N. \tag{35}$$

where

$$\boldsymbol{A}^{k,j+1}_j \equiv \begin{bmatrix} A^{k,j+1}_{1,j} \\ \vdots \\ A^{k,j+1}_{N,j} \end{bmatrix}, \qquad \boldsymbol{B}^k_j \equiv \begin{bmatrix} l_{1,j}[(1-\Theta)A^{k,j+1}_{0,j} + \Theta A^{k,j+1}_{0,j+1}] \\ 0 \\ \vdots \\ 0 \\ u_{N,j}[(1-\Theta)A^{k,j+1}_{N+1,j} + \Theta A^{k,j+1}_{N+1,j+1}] \end{bmatrix},$$

and, due to the definition of Arrow–Debreu securities,

$$\boldsymbol{A}^{k,j+1}_{j+1} = \begin{bmatrix} 0 \\ 0 \\ \vdots \\ 1 \\ \vdots \\ 0 \end{bmatrix} \leftarrow k\text{th row.}$$

The boundary matrix $\boldsymbol{B}^k_j$ in (35) cannot be related to market information, but must be specified directly through assumptions about the discretized branching process on the upper and lower x boundaries. If the finite-difference mesh spans a sufficient part of the relevant x space, the influence of $\boldsymbol{B}^k_j$ is generally negligible, and any reasonable assumption on local boundary behavior will suffice. For simplicity we will assume that both the upper and lower x boundaries are *absorbing*, i.e. for $l \geqslant j$,

$$A^{k,l}_{0,j} = \left\{ \begin{array}{ll} P_l/P_j & \text{if } k = 0 \\ 0 & \text{if } k = 1,\ldots,N+1 \end{array} \right\}, \qquad j = 0,\ldots,M, \tag{36a}$$

$$A^{k,l}_{N+1,j} = \left\{ \begin{array}{ll} P_l/P_j & \text{if } N+1 \\ 0 & \text{if } k = 0,\ldots,N \end{array} \right\}, \qquad j = 0,\ldots,M. \tag{36b}$$

In this case, the $N \times 1$ boundary matrix simplifies to $\boldsymbol{B}^k_j = \boldsymbol{0}$ $(k = 1,\ldots,N)$.

Let us now introduce the $N \times N$ matrices

$$\boldsymbol{A}^{j+1}_j = [\boldsymbol{A}^{1,j+1}_j,\ldots,\boldsymbol{A}^{N,j+1}_j], \qquad \boldsymbol{A}^{j+1}_{j+1} = [\boldsymbol{A}^{1,j+1}_{j+1},\ldots,\boldsymbol{A}^{N,j+1}_{j+1}], \qquad \boldsymbol{B}_j = [\boldsymbol{B}^1_j,\ldots,\boldsymbol{B}^N_j].$$

As $\boldsymbol{A}_{j+1}^{j+1}$ obviously equals the identity matrix and $\boldsymbol{B}_j$ is the zero-matrix (due to the assumption (36a, b)), (35) can be written compactly as

$$\left(\frac{P_j}{P_{j+1}}\boldsymbol{I} - (1-\Theta)\boldsymbol{M}_j\right)\boldsymbol{A}_j^{j+1} = \Theta\boldsymbol{M}_j + \boldsymbol{I}, \qquad j = 0, \ldots, M. \tag{37}$$

If, as justified earlier, we assume that $\Theta \neq 1$, this equation can alternatively be written (for $j = 0, \ldots, M$)

$$\boldsymbol{A}_j^{j+1} = \frac{-\Theta}{1-\Theta}\boldsymbol{I} + \left(\frac{P_j}{P_{j+1}}I - (1-\Theta)\boldsymbol{M}_j\right)^{-1}\left(\boldsymbol{I}\frac{\left(\Theta P_j/P_{j+1} + (1-\Theta)\right)}{1-\Theta}\right), \tag{38}$$

where we have assumed that $\left(P_j/P_{j+1}\boldsymbol{I} - (1-\Theta)\boldsymbol{M}_j\right)$ is invertible (see discussion in Appendix A).

To transform (38) into an equation involving the known (from (33a, c)) time-0 Arrow–Debreu prices, $A_{\text{ini}}^{i,j}$, we use the fact that

$$A_{\text{ini}}^{i,j+1} = \sum_{l=0}^{N+1} A_{\text{ini}}^{l,j} A_{l,j}^{i,j+1} = \sum_{l=1}^{N} A_{\text{ini}}^{l,j} A_{l,j}^{i,j+1}, \qquad i = 1, \ldots, N, \quad j = 0, \ldots, M, \tag{39}$$

where the second equality follows from the assumption of absorbing barriers, (36a, b). In matrix notation (39) is just

$$\left(\boldsymbol{A}_{\text{ini}}^{j+1}\right)^{\mathrm{T}} = \left(\boldsymbol{A}_{\text{ini}}^{j}\right)^{\mathrm{T}}\boldsymbol{A}_j^{j+1}, \qquad j = 0, \ldots, M, \tag{40}$$

where $\boldsymbol{A}_{\text{ini}}^{j}$ is a $N \times 1$ vector

$$\boldsymbol{A}_{\text{ini}}^{j} = \begin{bmatrix} A_{\text{ini}}^{1,j} \\ A_{\text{ini}}^{2,j} \\ \vdots \\ A_{\text{ini}}^{N,j} \end{bmatrix}.$$

Applying (40) to (38) yields a recursive relation in the initial Arrow–Debreu prices

$$\left(\boldsymbol{A}_{\text{ini}}^{j+1}\right)^{\mathrm{T}} = \frac{-\Theta}{1-\Theta}\left(\boldsymbol{A}_{\text{ini}}^{j}\right)^{\mathrm{T}} + \left(\boldsymbol{A}_{\text{ini}}^{j}\right)^{\mathrm{T}}\left(\frac{P_j}{P_{j+1}}\boldsymbol{I} - (1-\Theta)\boldsymbol{M}_j\right)^{-1}\left(\boldsymbol{I}\frac{\left(\Theta P_j/P_{j+1} + (1-\Theta)\right)}{1-\Theta}\right), \quad j = 0, \ldots, M. \tag{41}$$

Equation (41) is the discrete-time version of the Fokker–Planck equation (7). All terms in the equation are known except for the matrix $\boldsymbol{M}_j$ which depends on the unknown node volatilities $\hat{v}_{i,j}$. To solve for these volatilities, we rearrange (41) to

$$\left(\boldsymbol{M}_j\right)^{\mathrm{T}}\left((1-\Theta)\boldsymbol{A}_{\text{ini}}^{j+1} + \Theta\boldsymbol{A}_{\text{ini}}^{j}\right) = \left(P_j/P_{j+1}\right)\boldsymbol{A}_{\text{ini}}^{j+1} - \boldsymbol{A}_{\text{ini}}^{j}, \qquad j = 0, \ldots, M. \tag{42}$$

From (23a, c) and (30), we notice that $\left(\boldsymbol{M}_j\right)^{\mathrm{T}}$ can be decomposed into

$$\left(\boldsymbol{M}_j\right)^{\mathrm{T}} = \begin{bmatrix} -\alpha\hat{v}_{1,j} & U\hat{v}_{2,j} & 0 & 0 & 0 & \cdots & 0 \\ L\hat{v}_{1,j} & -\alpha\hat{v}_{2,j} & U\hat{v}_{3,j} & 0 & 0 & \cdots & 0 \\ 0 & L\hat{v}_{2,j} & -\alpha\hat{v}_{3,j} & U\hat{v}_{4,j} & 0 & \cdots & 0 \\ 0 & 0 & L\hat{v}_{3,j} & -\alpha\hat{v}_{4,j} & U\hat{v}_{5,j} & \cdots & 0 \\ \vdots & \vdots & \vdots & \vdots & \vdots & \cdots & 0 \\ 0 & 0 & 0 & \cdots & L\hat{v}_{N-2,j} & -\alpha\hat{v}_{N-1,j} & U\hat{v}_{N,j} \\ 0 & 0 & 0 & \cdots & 0 & L\hat{v}_{N-1,j} & -\alpha\hat{v}_{N,j} \end{bmatrix}$$
$$+ \begin{bmatrix} 0 & -\lambda_j & 0 & 0 & 0 & \cdots & 0 \\ \lambda_j & 0 & -\lambda_j & 0 & 0 & \cdots & 0 \\ 0 & \lambda_j & 0 & -\lambda_j & 0 & \cdots & 0 \\ 0 & 0 & \lambda_j & 0 & -\lambda_j & \cdots & 0 \\ \vdots & \vdots & \vdots & \vdots & \vdots & \cdots & 0 \\ 0 & 0 & 0 & \cdots & \lambda_j & 0 & -\lambda_j \\ 0 & 0 & 0 & \cdots & 0 & \lambda_j & 0 \end{bmatrix} \equiv \boldsymbol{V}_j + \boldsymbol{\Lambda}_j, \qquad j = 0, \ldots, M, \quad (43)$$

where

$$U = \tfrac{1}{2}\alpha\left(1 + \tanh\tfrac{1}{2}\Delta_x\right), \quad (44a)$$

$$L = \tfrac{1}{2}\alpha\left(1 - \tanh\tfrac{1}{2}\Delta_x\right), \quad (44b)$$

$$\lambda_j = \frac{1}{2\sinh\Delta_x}\left(\frac{P_j/P_{j+1} - \Gamma_j/\Gamma_{j+1}}{(1-\Theta) + \Theta\Gamma_j/\Gamma_{j+1}}\right). \quad (44c)$$

(43) and (42) can now, finally, be combined as a linear system of equations in the unknown volatilities

$$\boldsymbol{\Psi}_j\hat{\boldsymbol{v}}_j = \left(P_j/P_{j+1}\boldsymbol{A}_{\mathrm{ini}}^{j+1} - \boldsymbol{A}_{\mathrm{ini}}^{j}\right) - \Lambda_j\left((1-\Theta)\boldsymbol{A}_{\mathrm{ini}}^{j+1} + \Theta\boldsymbol{A}_{\mathrm{ini}}^{j}\right), \qquad j = 0, \ldots, M, \quad (45)$$

where $\boldsymbol{\Lambda}_j$ is defined in (43) and (44c),

$$\hat{\boldsymbol{v}}_j \equiv \begin{bmatrix} \hat{v}_{1,j} \\ \hat{v}_{2,j} \\ \vdots \\ \hat{v}_{N,j} \end{bmatrix},$$

and, with $\bar{\boldsymbol{A}}_{\mathrm{ini}}^{j} \equiv (1-\Theta)\boldsymbol{A}_{\mathrm{ini}}^{j+1} + \Theta\boldsymbol{A}_{\mathrm{ini}}^{j}$,

$$\boldsymbol{\Psi}_j \equiv \begin{bmatrix} -\alpha\bar{A}^{1,j}_{\text{ini}} & U\bar{A}^{2,j}_{\text{ini}} & 0 & 0 & 0 & \cdots & 0 \\ L\bar{A}^{1,j}_{\text{ini}} & -\alpha\bar{A}^{2,j}_{\text{ini}} & U\bar{A}^{3,j}_{\text{ini}} & 0 & 0 & \cdots & 0 \\ 0 & L\bar{A}^{2,j}_{\text{ini}} & -\alpha\bar{A}^{3,j}_{\text{ini}} & U\bar{A}^{4,j}_{\text{ini}} & 0 & \cdots & 0 \\ 0 & 0 & L\bar{A}^{3,j}_{\text{ini}} & -\alpha\bar{A}^{4,j}_{\text{ini}} & U\bar{A}^{5,j}_{\text{ini}} & \cdots & 0 \\ \vdots & \vdots & \vdots & \vdots & \vdots & \cdots & 0 \\ 0 & 0 & 0 & \cdots & L\bar{A}^{N-2,j}_{\text{ini}} & -\alpha\bar{A}^{N-1,j}_{\text{ini}} & U\bar{A}^{N,j}_{\text{ini}} \\ 0 & 0 & 0 & \cdots & 0 & L\bar{A}^{N-1,j}_{\text{ini}} & -\alpha\bar{A}^{N,j}_{\text{ini}} \end{bmatrix}.$$

In principle, determination of node volatilities can now be done by solving the simple tridiagonal system (45) for all $j = 0, \ldots, M$. As it turns out, however, (45) must be applied with some care due to the sometimes very low magnitude of the elements in the boundaries of the matrices of (45). For options maturing at low values of t_j, the extremely low likelihood of S reaching either the upper or lower x boundaries within $(0, t_j]$ makes it difficult to determine the short-term volatility function for values of x close to the upper and lower boundaries in the mesh. For pricing purposes, this is largely irrelevant as the sensitivity (vega) of all realistic options to the extreme upper and lower edges of the short-term volatility function is virtually nonexistent. To avoid numerical problems in (45), for each time-step t_j one could limit the application of the equation to the statistically significant part of x-space (see Figure 1 and Endnote 5) and truncate off irrelevant rows and columns of the matrices in (45). Volatilities in discarded regions of the mesh could, for example, be set to some appropriate constant.

In a direct solution of (45) (after truncation), it is not unlikely that small imperfections and arbitrage opportunities in the input data will lead to spikes in local volatilities and even, occasionally, might cause some $\hat{v}$'s to become negative. At the sacrifice of overall speed, we can, for example, overcome such problems by

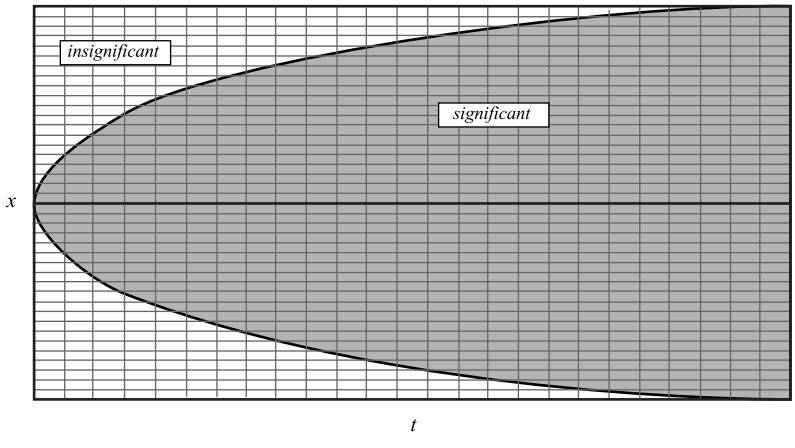

FIGURE 1

imposing smoothness and value constraints on the $\hat{v}$'s. As a simple example of such regularization techniques, consider limiting the vector $\hat{\boldsymbol{v}}_j$ to the bounds $\hat{\boldsymbol{v}}_{\min} \leqslant \hat{\boldsymbol{v}}_j \leqslant \hat{\boldsymbol{v}}_{\max}$ and replacing equation (45) by the minimization of a quadratic form. With the short notation

$$\boldsymbol{T}_j = -\left(P_j/P_{j+1}\boldsymbol{A}_{\text{ini}}^{j+1} - \boldsymbol{A}_{\text{ini}}^{j}\right) + \boldsymbol{\Lambda}_j\left((1-\Theta)\boldsymbol{A}_{\text{ini}}^{j+1} + \Theta\boldsymbol{A}_{\text{ini}}^{j}\right), \tag{46}$$

(45) reduces to

$$\boldsymbol{\Psi}_j\hat{\boldsymbol{v}}_j + \boldsymbol{T}_j = 0, \qquad j = 0, \ldots, M,$$

which suggests the following quadratic program (for $j = 0, \ldots, M$)

$$\begin{aligned} &\text{Minimize} && \left(\boldsymbol{\Phi}_j\left(\boldsymbol{\Psi}_j\hat{\boldsymbol{v}}_j + \boldsymbol{T}_j\right)\right)^{\mathrm{T}}\left(\boldsymbol{\Phi}_j\left(\boldsymbol{\Psi}_j\hat{\boldsymbol{v}}_j + \boldsymbol{T}_j\right)\right) \\ &\text{subject to} && \hat{\boldsymbol{v}}_{\min} \leqslant \hat{\boldsymbol{v}}_j \leqslant \hat{\boldsymbol{v}}_{\max}, \end{aligned} \tag{47}$$

where $\boldsymbol{\Phi}_j$ is some[10] appropriate $N \times N$ scaling matrix, and $\hat{\boldsymbol{v}}_{\min}$ and $\hat{\boldsymbol{v}}_{\max}$ are $N \times 1$ vectors containing the specified lower and upper constraints on the volatility vector. We note that if $\boldsymbol{\Psi}_j$ is invertible and none of the constraints binding, the solution to the quadratic program (47) will exactly equal the solution to (45). (47) can be written in canonical form as follows (for $j = 0, \ldots, M$):

$$\begin{aligned} &\text{Minimize} && \tfrac{1}{2}\left(\boldsymbol{y}_j\right)^{\mathrm{T}}\boldsymbol{Q}_j\boldsymbol{y}_j + \left(\boldsymbol{c}_j\right)^{\mathrm{T}}\boldsymbol{y}_j \\ &\text{subject to} && 0 \leqslant \boldsymbol{y}_j \leqslant \boldsymbol{y}_{\max}, \end{aligned} \tag{48}$$

where

$$\begin{aligned} \boldsymbol{y}_j &= \hat{\boldsymbol{v}}_j - \hat{\boldsymbol{v}}_{\min}, \\ \boldsymbol{y}_{\max} &= \hat{\boldsymbol{v}}_{\max} - \hat{\boldsymbol{v}}_{\min}, \\ \boldsymbol{Q}_j &= \left(\boldsymbol{\Phi}_j\boldsymbol{\Psi}_j\right)^{\mathrm{T}}\left(\boldsymbol{\Phi}_j\boldsymbol{\Psi}_j\right) \\ \left(\boldsymbol{c}_j\right)^{\mathrm{T}} &= \left(\boldsymbol{T}_j + \boldsymbol{\Psi}_j\boldsymbol{v}_{\min}\right)^{\mathrm{T}}\left(\Phi_j\right)^{\mathrm{T}}\boldsymbol{\Phi}_j\boldsymbol{\Psi}_j. \end{aligned}$$

Notice that $\boldsymbol{Q}_j$ by construction is a positive-definite real symmetric matrix. This fact allows us to solve the canonical quadratic program with Lemke's method (see e.g. Ecker and Kupferschmid 1988: Chap. 9), a simple efficient algorithm that only involves pivot operations on the matrices in (48).

With (48), the specification of the implicit and semi-implicit finite-difference algorithms is complete. We summarize the complete algorithm in the following proposition.

Proposition 2. The finite-difference solution to the valuation equation (17) is given by the tridiagonal matrix equation (22). Requiring that the finite-difference mesh correctly prices (i) zero coupon bonds; (ii) asset forward contracts; and (iii) European call options, the matrices in (22) are determined by equations (26), (30), (33a, d), and (45). To avoid numerical problems due to boundary-effects and flaws in the input data, (45) can, for example, be replaced by the quadratic program (47)–(48).

4. EXAMPLES AND TESTS

The first challenge in the application of the algorithm concerns the collection of bond, stock, and call option data to span the entire finite-difference mesh. Whereas normally sufficient zero-coupon rates and stock dividends can be constructed from market data, the available call price data are typically limited to relatively few different strikes and maturities. To overcome the lack of call price data, it is necessary to introduce both interpolation and extrapolation techniques.

To focus on a specific example, consider the following matrix (Table 1) of implied Black–Scholes volatilities, $\theta(K, T)$, on European call options on the S&P 500 index (October 1995).

The short-term volatilities ($T < 1$ year) could be obtained from exchange-traded options; longer maturities must be sampled from the over-the-counter broker markets. In practice some entries of Table 1 are not directly available in the market, in which case interpolation/extrapolation techniques are needed to complete the grid. In particular, the upper right-hand corner (short maturities, high strikes) is typically not quoted in the market. In our example, we have chosen an exaggerated upward-sloping smile in this section of the volatility table (see Figure 2). While not realistic, the resulting curve shape puts stress on the numerical algorithm and as such is a good basis for testing. In specification of tables like the one above, we point out that one must generally be quite careful about the behavior of implied volatilities for large T (say, $T > 4$–5 years). Specifically, the central limit theorem suggests that the volatility smile should gradually flatten out as maturity is increased. If one blindly extrapolates volatility data from short-term options to long-term options, arbitrages are likely to arise (which will be reflected in local volatilities that become unstable for large T).

TABLE 1. Implied volatilities of S&P 500 equity index.

	Strike K (% of spot)									
T \ K =	85%	90%	95%	100%	105%	110%	115%	120%	130%	140%
0.175	0.190	0.168	0.133	0.113	0.102	0.097	0.120	0.142	0.169	0.200
0.425	0.177	0.155	0.138	0.125	0.109	0.103	0.100	0.114	0.130	0.150
0.695	0.172	0.157	0.144	0.133	0.118	0.104	0.100	0.101	0.108	0.124
0.940	0.171	0.159	0.149	0.137	0.127	0.113	0.106	0.103	0.100	0.110
1.000	0.171	0.159	0.150	0.138	0.128	0.115	0.107	0.103	0.099	0.108
1.500	0.169	0.160	0.151	0.142	0.133	0.124	0.119	0.113	0.107	0.102
2.000	0.169	0.161	0.153	0.145	0.137	0.130	0.126	0.119	0.115	0.111
3.000	0.168	0.161	0.155	0.149	0.143	0.137	0.133	0.128	0.124	0.123
4.000	0.168	0.162	0.157	0.152	0.148	0.143	0.139	0.135	0.130	0.128
5.000	0.168	0.164	0.159	0.154	0.151	0.148	0.144	0.140	0.136	0.132

In the design of a scheme to interpolate between cells in Table 1,[11] we notice from (16) that such a scheme must be smooth enough to ensure that $\partial\theta/\partial T$, $\partial\theta/\partial K$, and $\partial^2\theta/\partial K^2$ are well behaved. One interpolation approach suggested in the literature (Shimko 1993, Barle and Cakici 1995) involves a parabolic regression on the data in (K, T) table. If exact reproduction of all table entries is desired, various spline-based schemes can be applied (Press *et al.* 1992: Chap. 3; Dierckx 1995: Chap. 2).

In the pricing of long-term options, capturing the statistically significant S-space in a finite-difference mesh would involve setting the S-boundary conditions much further apart than the 85–140% strike range covered by Table 1. The necessary extrapolation of the data in Table 1 to span the entire finite-difference mesh can be done in a multitude of ways dependent on what view is held about future stock price behavior. Shimko (1993) performs this extrapolation by grafting log-normal tails to the Arrow–Debreu profiles[12] constructed from (33a, d); Rubinstein (1994), on the other hand, uses a nonlinear optimization technique to minimize the deviation of the total Arrow–Debreu profile from that of a perfectly log-normal distribution. Further approaches are suggested in Jackwerth and Rubinstein (1996), and Andreasen (1996). We do not endorse any particular approach, but do caution that simply flattening out the volatility curve outside the upper and lower strikes in Table 1 will introduce large spikes in both $\partial\theta/\partial K$ and $\partial^2\theta/\partial K^2$ that can adversely affect the quality of the volatility smile fit.

Let us now consider pricing 2-year European call options in the presence of the volatility smile in Table 1. We will use the market data

$$S_{\text{ini}} = \$590, \qquad r = 6\%, \qquad \gamma = 2.62\%$$

together with the mesh parameters[13]

$$\Theta = 0.5 \quad \text{(Crank–Nicholson)}, \qquad T = 2, \qquad N = 65, \qquad M = 25,$$

$$S_0 = \$195.65 \quad \Rightarrow \quad x_0 = 5.276, \qquad S_{66} = \$1906.22 \quad \Rightarrow \quad x_{66} = 7.553.$$

The mesh lines up with the initial stock price, $S_{32} = S_{\text{ini}} = \$590$ (that is, $\beta = 32$).

To interpolate in Table 1, we here apply the simple bicubic splines suggested in Press *et al.* (1992: Chap. 2). In this approach, cubic splines are fit to all T columns of the (K, T)-table whereafter a second cubic spline is fit along the K direction. While adequate for our example, we notice that the bicubic scheme suffers from the drawback that smoothness is only guaranteed in the K direction. More sophisticated spline interpolation schemes that are smooth in both T and K directions are discussed in Dierckx (1995). Application of bicubic spline interpolation combined with a smooth, gradual flattening of the volatility curve outside the limits of Table 1 yield implied volatilities in the mesh as depicted in Figure 2.

Applying the Black–Scholes pricing equation (9) and using the result (33a, d), we get the following time-0 Arrow–Debreu prices in the mesh (Figure 3).

Given the Arrow–Debreu profiles, we can now use Lemke's method on (48) to construct the local volatilities in the mesh. We constrain the magnitude of the local

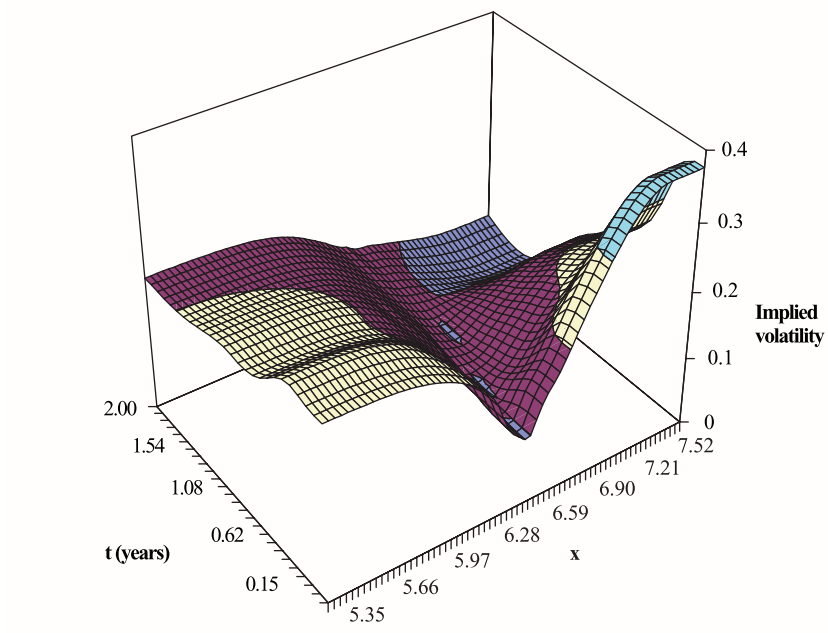

FIGURE 2. Implied volatilities in 2-year finite-difference mesh: $S_{\text{ini}} = \$590$, $r = 6\%$, $\gamma = 2.62\%$, $N = 65$, $M = 25$.

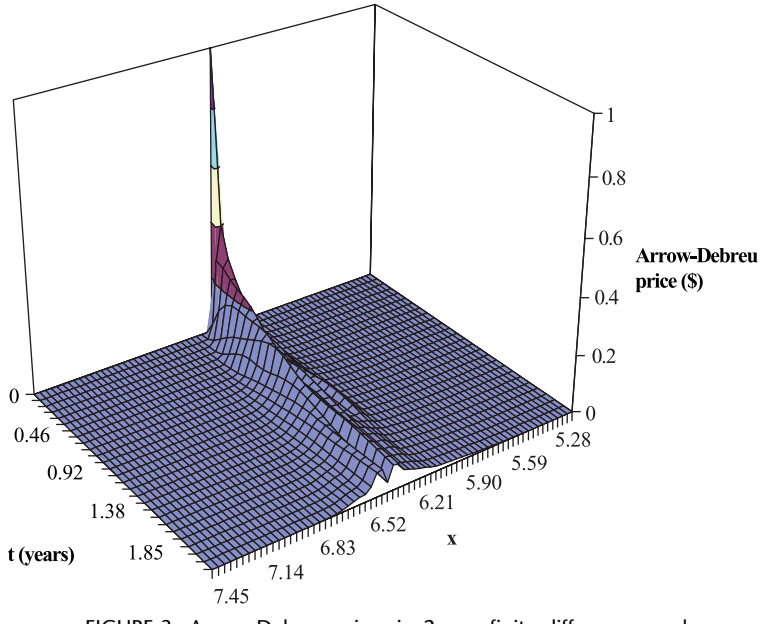

FIGURE 3. Arrow–Debreu prices in 2-year finite-difference mesh: $S_{\text{ini}} = \$590$, $r = 6\%$, $\gamma = 2.62\%$, $N = 65$, $M = 25$.

volatilities to the interval (0.04, 0.4), i.e.

$$\hat{\boldsymbol{v}}_{\max} = \begin{bmatrix} 0.16 \\ 0.16 \\ \vdots \\ 0.16 \end{bmatrix}, \qquad \hat{\boldsymbol{v}}_{\min} = \begin{bmatrix} 0.0016 \\ 0.0016 \\ \vdots \\ 0.0016 \end{bmatrix}.$$

To speed up this calculation, we have limited the optimization to part of the mesh that has a significant contribution to (48); volatilities outside of this area have been (arbitrarily) set to 0.20.

Notice that the local volatility surface is considerably less smooth than the implied volatilities in Figure 2. This is not surprising as local volatilities are, in effect, generated from time- and strike-derivatives of the implied volatility surface (see (16)). Many of the spikes in the surface above can be attributed to the lack of control over the T-derivative in our bicubic interpolation scheme. As mentioned earlier, the smoothness of the volatility surface can be improved by using either a more sophisticated spline scheme (perhaps allowing for some bid–offer slack in the quoted prices) or, at a loss of accuracy, a regression approach[14] (as in Shimko 1993). We do point out, however, that localized spikes in the local volatility surface typically will have very limited impact on option prices. Also, the quadratic optimization approach (48) with its built-in constraints on local volatility will act as a smoothing device and will ensure that any spikes do not get too large.

Having now determined the local volatility function, we are ready to apply the finite-difference scheme (22) (combined with (26) and (30)) to contingent claims pricing. For call options, the appropriate boundary conditions in the finite-difference mesh are

$$\begin{aligned} H_{0,j} &= \$0, \qquad j = 0, \ldots, 26, \\ H_{66,j} &= S_{66} \exp[-\gamma(T - t_j)] - K \exp[-r(T - t_j)], \qquad j = 0, \ldots, 26, \\ H_{i,26} &= \max(S_i - K, 0) = \max(\mathrm{e}^{x_i} - K, 0), \qquad i = 1, 2, \ldots, 65. \end{aligned}$$

Using these conditions to set the vectors $\boldsymbol{B}_j$ and $\boldsymbol{H}_{26}$ in (22), we solve backwards through the mesh to find $\boldsymbol{H}_0$; the current value of the option can be picked out as the 32nd row of $\boldsymbol{H}_0$. The results are summarized in Table 2.

With a maximum pricing error of around 5 cents (or, in terms of implied volatility, around 0.0003) and an average error of less than 2 cents, the Crank–Nicholson method excellently reproduces actual call option prices across the full range of strikes. The time needed to compute Table 2 was 4.7 seconds on a DEC Alpha 8400 5/300 mini-computer[15] (4.3 seconds to compute the local volatilities and 0.4 seconds to price the options). We have repeated the above calculations for all option maturities and strikes in Table 1 using grid sizes varying from $M = 10$ and $N = 50$ ($T = 0.175$) to $M = 40$ and $N = 100$ ($T = 10$); the maximum absolute price error amounted to 7.3 cents and occurred for $T = 0.940$ and $K = 85\%$ (the total value of this option is \$106.782).

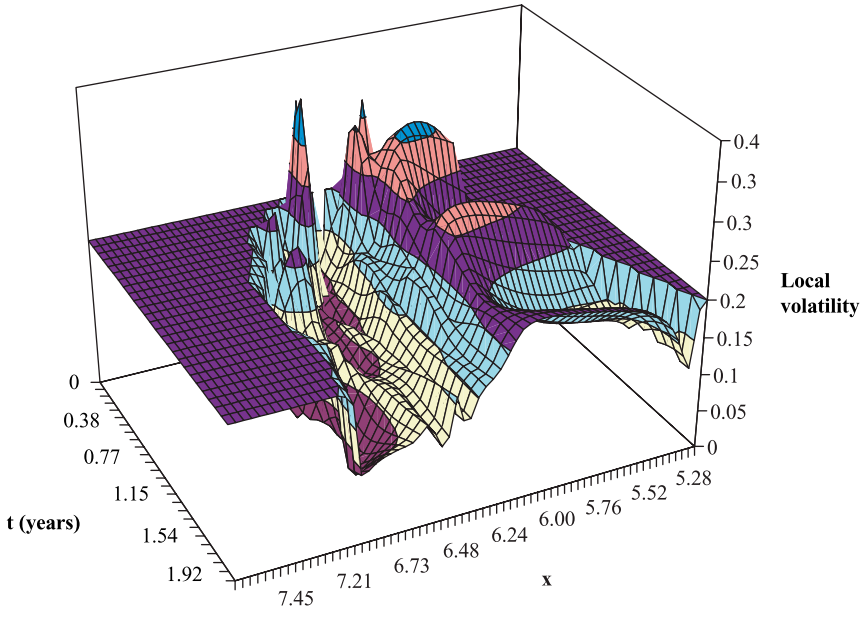

FIGURE 4. Local instantaneous volatilities in 2-year finite-difference mesh: $S_{ini} = \$590$, $r = 6\%$, $\gamma = 2.62\%$, $N = 65$, $M = 25$.

Having verified that our algorithm accurately reproduces the volatility smile, we now turn to the pricing of knock-out options. Due to their path-dependency, these contracts require a complete intertemporal description of the volatility smile throughout the life of the option and are consequently a good test of the full potential of our

TABLE 2. Two-year call option prices by Crank–Nicholson finite-difference algorithm ($S_{ini} = \$590$, $r = 6\%$, $\gamma = 2.62\%$, $N = 65$, $M = 25$).

Strike (% spot)	Implied volatility	Black–Scholes theoretical price	Finite-difference price	Finite-difference implied vol.	Price error (cents)	Volatility error
85	0.169	\$125.7022	\$125.7490	0.16927	¢4.68	0.000 27
90	0.161	\$103.9506	\$103.9617	0.16105	¢1.11	0.000 05
95	0.153	\$83.5822	\$83.6181	0.15314	¢3.59	0.000 14
100	0.145	\$64.8986	\$64.9016	0.14501	¢0.30	0.000 01
105	0.137	\$48.2225	\$48.2453	0.13707	¢2.28	0.000 07
110	0.130	\$34.1869	\$34.1981	0.13004	¢1.12	0.000 04
115	0.126	\$23.6128	\$23.6186	0.12602	¢0.58	0.000 02
120	0.119	\$14.6757	\$14.6852	0.11904	¢0.95	0.000 04
130	0.115	\$5.6466	\$5.6507	0.11502	¢0.41	0.000 02
140	0.111	\$1.7779	\$1.7821	0.11105	¢0.42	0.000 05

finite-difference approach.[16] Using the market data above, we will first consider a 2-year at-the-money down-and-out call on the S&P 500 with a knock-out level of $H = \$530$. As discussed in Section 1, to ensure rapid convergence we must make sure that the x grid is always aligned perfectly with the barrier, i.e. $x_\varphi = \ln(530)$ for some integer $\varphi \in (0, M+1)$. The boundary conditions of the down-and-out knock-out are then as follows

$$H_{i,j} = \$0, \qquad i = 0, \ldots, \varphi, \quad j = 0, \ldots, M+1,$$

$$H_{N+1,j} = S_{N+1} \exp[-\gamma(T - t_j)] - K \exp[-r(T - t_j)], \qquad j = 0, \ldots, M+1,$$

$$H_{i,M+1} = \max(S_i - K, 0) = \max(e^{x_i} - K, 0), \qquad i = 1, 2, \ldots, N.$$

Using various values of N and M (and thus various values of Δ_t and Δ_x) in a Crank–Nicholson finite-difference scheme yields the option prices shown in Table 3.

Unlike methods based on binomial lattices (see Boyle and Lau 1994)), the convergence of the finite-difference method is perfectly smooth in both Δ_t and Δ_x. Moreover, the convergence of option prices is quite fast in both Δ_t and Δ_x; in fact, all numbers in the table are within 0.32% (or 17 cents) of the \$52.286 value obtained at the highest mesh resolution of $N = 150$ and $M = 45$.

In addition to the option price, Table 3 also contains an implied volatility; this number is defined as a (constant) volatility that equates the standard Rubinstein–Reiner knock-out pricing formula (see Rubinstein and Reiner 1991) with the pricing result

TABLE 3. Two-year knock-out prices and implied volatilities by Crank–Nicholson ($S_{\text{ini}} = K = \$590, H = \$530, r = 6\%, \gamma = 2.62\%$).

M	$N = 40$ $\Delta_x = 0.054$	$N = 60$ $\Delta_x = 0.036$	$N = 80$ $\Delta_x = 0.027$	$N = 100$ $\Delta_x = 0.021$	$N = 120$ $\Delta_x = 0.018$	$N = 150$ $\Delta_x = 0.015$
5	\$52.204 65 0.123 411	\$52.297 15 0.124 351	\$52.323 25 0.124 619	\$52.335 29 0.124 743	\$52.337 62 0.124 771	\$52.338 02 0.124 771
10	\$52.135 20 0.122 715	\$52.235 28 0.123 721	\$52.267 31 0.124 046	\$52.283 85 0.124 215	\$52.290 79 0.124174	\$52.289 43 0.124257
15	\$52.124 09 0.122 604	\$52.227 79 0.123 645	\$52.263 89 0.124 012	\$52.279 85 0.124 174	\$52.287 96 0.124 257	\$52.28639 0.124 241
20	\$52.122 80 0.122 592	\$52.226 43 0.123 631	\$52.263 19 0.124 004	\$52.279 41 0.124 170	\$52.287 02 0.124 248	\$52.286 50 0.124 242
25	\$52.122 41 0.122 588	\$52.225 43 0.123 621	\$52.261 76 0.123 99	\$52.279 22 0.124 168	\$52.286 68 0.124 244	\$52.285 59 0.124 233
30	\$52.121 70 0.122 581	\$52.226 09 0.123 628	\$52.262 49 0.123 997	\$52.278 54 0.124 161	\$52.286 80 0.124 245	\$52.286 77 0.124 245
35	\$52.120 88 0.122 572	\$52.226 19 0.123 629	\$52.262 01 0.123 992	\$52.278 08 0.124 156	\$52.286 21 0.124 239	\$52.286 88 0.124 246
45	\$52.120 08 0.122 565	\$52.225 94 0.123 626	\$52.261 04 0.123 983	\$52.277 38 0.124 149	\$52.285 96 0.124 237	\$52.286 37 0.124 241

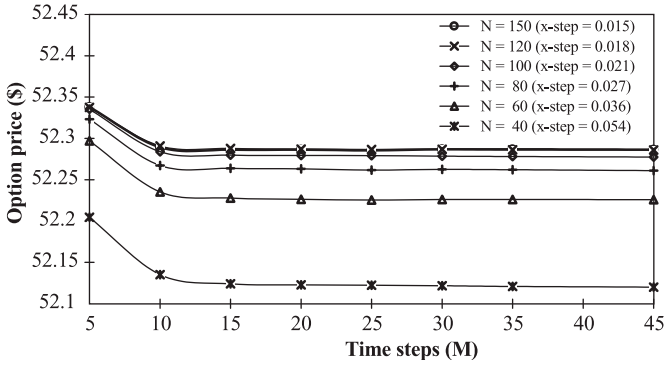

FIGURE 5. Convergence profiles for 2-year down-and-out knock-out option: $S_{ini} = K = \$590$, $H = \$530$, $r = 6\%$, $\gamma = 2.62\%$.

generated by the finite-difference mesh. In our example, the implied volatility is around 0.124 which is significantly lower than both the at-the-money implied call volatility (0.145) and the implied volatility of a call option with a strike equal to the \$530 knock-out barrier (around 0.161).

To further investigate the implied volatility of knock-out options, consider now again a 2-year at-the-money knock-out option. We set $N = 100$ and $M = 30$ and leave market data unchanged from the previous examples. Dependent on the knock-out level H, option prices and implied volatilities are as shown in Table 4.

Interestingly, for knock-out levels in the region around \$540–\$555 the calculated option prices are consistent with *two* implied volatilities. This phenomenon is caused by the fact that knock-out option prices, unlike prices of regular calls and puts, can be bounded, nonmonotonic functions of implied volatility (see Figure 6). It is not

TABLE 4. Two-year knock-out prices and implied volatilities by Crank–Nicholson finite-difference method ($S_{ini} = K = \$590, r = 6\%, \gamma = 2.62\%, N = 100, M = 30$).

Barrier H	Price	Implied volatility
\$500	\$59.5867	0.133 49
\$510	\$57.7751	0.130 95
\$520	\$55.3933	0.127 93
\$530	\$52.2785	0.124 16
\$540	\$48.2554	0.119 02 or 1.609 91
\$550	\$43.0306	0.098 87 or 0.157 30
\$555	\$39.8444	0.059 63 or 0.127 47
\$560	\$36.2468	0.120 04
\$570	\$27.4257	0.112 79

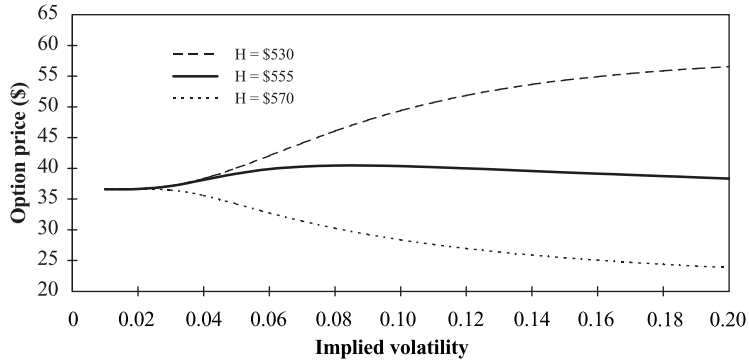

FIGURE 6. Down-and-out knock-out option prices as a function of implied volatility: $S_{\text{ini}} = K = \$590$, $r = 6\%$, $\gamma = 2.62\%$.

inconceivable that certain volatility smiles can give rise to knock-out option prices that are not consistent with any implied volatility in the Black–Scholes environment. The concept of implied volatility of knock-out options should, in general, be approached with care.

5. CONCLUSIONS AND EXTENSIONS

In this paper we have developed and tested an algorithm to incorporate volatility smiles in the construction of implicit and semi-implicit (Crank–Nicholson) finite-difference lattices. Based on the technique of forward induction, the algorithm is fast, accurate and extremely flexible. Although more complicated to implement than the standard implied binomial tree, the significant improvements in convergence properties and local branching behavior easily compensate for the additional implementation efforts.

In the paper, we have illustrated how our algorithm can be applied to price regular and knock-out calls, but many other applications are possible. As discussed in Dewynne and Wilmott (1993), the finite-difference method is capable of pricing a large number of exotic options, including American (or Bermudan) options, digital options, lookback options, Asian options, etc. To price options that are too complicated for the regular finite-difference method (e.g. certain classes of strongly path-dependent options), we can use a simulation approach where paths are randomly drawn through the lattice in accordance with the pseudo-probabilities given by equation (38). Alternatively, and more simply, we can use the computed instantaneous volatility surface directly in a regular Monte Carlo scheme.

Finally, we point out that our general approach of incorporating forward induction in the Crank–Nicholson and implicit finite-difference methods should prove useful in many applications other than fitting of volatility smiles. One such application is the

calibration of short-rate interest rate models to market data which is normally performed either by binomial trees (Jamshidian 1991) or by modified explicit finite-difference schemes (Hull and White 1994).

REFERENCES

Andreasen, J., Implied modelling: stable implementation, hedging, and duality, Working Paper, University of Aarhus, 1996.

Arnold, L., *Stochastic Differential Equations: Theory and Practice*, John Wiley & Sons, 1974.

Avallaneda M., C. Friedman, R. Holmes, and D. Samperi, Calibrating volatility surfaces via relative-entropy minimization, Working Paper, Courant Institute, New York University, 1996.

Barle, S. and N. Cakici, Growing a smiling tree, *Risk* (October 1995), 76–81.

Black, F. and M. Scholes, The pricing of options and other corporate liabilities, *Journal of Political Economy*, **81** (May–June 1973), 637–659.

Beckers, S., The constant elasticity of variance model and its implications for options pricing, *Journal of Finance*, **35** (1980), 661–673.

Boyle, P. and S. Lau, Bumping up against the barrier with the binomial method, *Journal of Derivatives*, **4** (1994), 6–14.

Breeden, D. and R. Litzenberger, Prices of state-contingent claims implicit in options prices, *Journal of Business*, **51** (October 1978), 621–651.

Brennan, M. and E. Schwartz, Finite difference methods and jump processes arising in the pricing of contingent claims: a synthesis, *Journal of Financial and Quantitative Analysis*, **13** (September 1978), 462–474.

Brown, G. and K. Toft, Constructing binomial trees from multiple implied probability distributions, Working Paper, University of Texas at Austin, 1996

Chriss, N., Transatlantic trees, *Risk* (July 1996), 45–48.

Courtadon, G., A more accurate finite difference approximation for the valuation of options, *Journal of Financial and Quantitative Analysis*, **17** (1982), 697–705.

Cox, D. and H. Miller, *The Theory of Stochastic Processes*, Chapman and Hall, 1965.

Cox, J. and S. Ross, The valuation of options for alternative stochastic processes, *Journal of Financial Economics*, **3** (March 1976), 145–166.

Derman, E. and I. Kani, Riding on a smile, *Risk* (February 1994), 32–39.

Derman, E., I. Kani, and N. Chriss, Implied trinomial trees of the volatility smile, Working Paper, Goldman Sachs, 1996.

Dewynne, J. and P. Wilmott, Partial to the exotic, *Risk* (March 1993), 38–46.

Dewynne, J., S. Howison, and P. Wilmott, *Option Pricing*, Oxford Financial Press, 1993.

Dierckx, P., *Curve and Surface Fitting with Splines*, Oxford Science Publications, 1995.

Dupire, B., Pricing with a smile, *Risk* (January 1994), 18–20.

Ecker, J. and M. Kupferschmid, *Introduction to Operations Research*, John Wiley & Sons, 1988.

Geske, R. and K. Shastri, Valuation of approximation: a comparison of alternative approaches, *Journal of Financial and Quantitative Analysis*, **20** (March 1985), 45–72.

Hull, J. and A. White, The pricing of options on assets with stochastic volatilities, *Journal of Finance*, **3** (1987), 281–300.

Hull, J. and A. White, Valuing derivative securities using the explicit finite difference method, *Journal of Financial and Quantitative Analysis*, **25** (March 1990), 87–100

Hull, J and A. White, Numerical procedures for implementing term structure models I: Single-factor models, *Journal of Derivatives*, **1** (Fall 1994), 7–16.

Jackwerth, J., Generalized binomial trees, Working Paper, University of California at Berkeley, 1996.

Jackwerth, J. and M. Rubinstein, Recovering probability distributions from option prices, *Journal of Finance*, **51** (December 1996), 1611–1631.

Jamshidian, F., Forward induction and construction of yield curve diffusion models, *Journal of Fixed Income*, **1** (June 1991), 62–74.

Karatzas, I. and S. Shreve, *Brownian Motion and Stochastic Calculus*, Springer Verlag, 1991.

Lagnado, R. and S. Osher, Reconciling differences, *Risk* (April 1997), 79–83.

Merton, R., Theory of rational option pricing, *Bell Journal of Economics and Management Science,* **4** (Spring 1973), 141–183.

Merton, R., Option pricing when underlying stock returns are discontinuous, *Journal of Financial Economics*, **3** (1976), 124–144.

Platen, E. and M. Schweizer, On smile and skewness, Working Paper, School of Mathematical Sciences, Australian National University, 1994.

Press, W., S. Teukolsky, W. Vetterling and B. Flannery, *Numerical Recipes in C*, Cambridge University Press, 1992.

Rubinstein, M., Nonparametric tests of alternative option pricing models using all reported trades and quotes on the 30 most active CBOE option classes from August 13, 1976, through August 31, 1978, *Journal of Finance*, **40** (June 1985), 455–480.

Rubinstein, M., Implied binomial trees, *Journal of Finance*, **49** (July 1994), 771–818.

Rubinstein, M., As simple as 1-2-3, *Risk* (January 1995), 44–47.

Rubinstein, M. and E. Reiner, Breaking down the barriers, *Risk* (September 1991), 28–35.

Shimko, D., Bounds of probability, *Risk* (April 1993), 33–37.

Zvan, R., P. Forsyth, and K. Vetzal, PDE methods for pricing barrier options, Working Paper, University of Waterloo, 1997

APPENDICES

Appendix A. Sufficient conditions for invertibility of (22)

In (22), consider the tridiagonal matrix

$$(1 + \hat{r}_j \Delta_t)\boldsymbol{I} - (1 - \Theta)\boldsymbol{M}_j.$$

It is well-known that a sufficient condition for a tridiagonal matrix to be invertible is that it is *diagonally dominant*, i.e. the absolute value of the diagonal element in each

row is strictly larger than the sum of the absolute values of the non-diagonal elements. For the matrix above, this translates into the condition (for $i = 1, \ldots, N$, $j = 0, \ldots, M$)

$$|1 + \hat{r}_j\Delta_t + (1-\Theta)\alpha\hat{v}_{i,j}| > \tfrac{1}{2}(1-\Theta)\big(|\alpha(\hat{v}_{i,j} + \Delta_x\hat{b}_{i,j})| + |\alpha(\hat{v}_{i,j} - \Delta_x\hat{b}_{i,j})|\big). \quad \text{(A.1)}$$

Using equation (30), we can write the right-hand-side (RHS) of the above inequality as

$$\text{RHS} = \tfrac{1}{2}(1-\Theta)(|A+B| + |C-B|),$$

where

$$A \equiv \alpha\hat{v}_{i,j}(1 - \tanh\tfrac{1}{2}\Delta_x), \qquad B \equiv \frac{(\hat{r}_j - \hat{\gamma}_j)\Delta_t}{\sinh\Delta_x(1+\Theta\hat{\gamma}_j\Delta_t)}, \qquad C \equiv \alpha\hat{v}_{i,j}(1 + \tanh\tfrac{1}{2}\Delta_x),$$

and $1 + \hat{\gamma}_j\Delta_t = \Gamma_j/\Gamma_{j+1}$.

As we require that $\hat{r}_j \geqslant 0$, $\hat{\gamma}_j \geqslant 0$ and $\hat{v}_{i,j} \geqslant 0$, both A and C are strictly positive (as $\Delta_x > 0$). B is positive or negative depending on the magnitude of $\hat{r}_j$ relative to $\hat{\gamma}_j$. Hence

$$\hat{r}_j \geqslant \hat{\gamma}_j: \quad \text{RHS} = \tfrac{1}{2}(1-\Theta)\max(A + C, 2B - C + A),$$
$$\hat{r}_j < \hat{\gamma}_j: \quad \text{RHS} = \tfrac{1}{2}(1-\Theta)\max(A + C, 2|B| + C - A).$$

Now, $(1-\Theta)(A+C)/2 = (1-\Theta)\alpha\hat{v}_{i,j}$, which is always less than the left-hand-side of (A.1). As $C - A > 0 > A - C$, a sufficient condition for inequality (A.1) to hold, irrespective of the sign of $\hat{r}_j - \hat{\gamma}_j$, is thus (for $i = 1, \ldots, N$, $j = 0, \ldots, M$)

$$1 + \hat{r}_j\Delta_t + (1-\Theta)\alpha\hat{v}_{i,j} > (1-\Theta)\left(\alpha\hat{v}_{i,j}\tanh\tfrac{1}{2}\Delta_x + \frac{|\hat{r}_j - \hat{\gamma}_j|\Delta_t}{\sinh\Delta_x(1+\Theta\hat{\gamma}_j\Delta_t)}\right),$$

or

$$1 + \hat{r}_j\Delta_t + (1-\Theta)\alpha\hat{v}_{i,j}(1 - \tanh\tfrac{1}{2}\Delta_x) > \frac{(1-\Theta)|\hat{r}_j - \hat{\gamma}_j|\Delta_t}{\sinh\Delta_x(1+\Theta\hat{\gamma}_j\Delta_t)}. \quad \text{(A.2)}$$

If we wish (A.2) to hold for all $\hat{v}_{i,j} \geqslant 0$ (unconditional invertibility), we must require that

$$1 + \hat{r}_j\Delta_t > \frac{(1-\Theta)|\hat{r}_j - \hat{\gamma}_j|\Delta_t}{\sinh\Delta_x(1+\Theta\hat{\gamma}_j\Delta_t)}, \qquad j = 0, \ldots, M. \quad \text{(A.3)}$$

To simplify, we note that a sufficient condition for (A.3) to hold is obviously

$$1 + \hat{r}_j\Delta_t > \frac{(1-\Theta)|\hat{r}_j - \hat{\gamma}_j|\Delta_t}{\Delta_x}, \qquad j = 0, \ldots, M. \quad \text{(A.4)}$$

To turn (A.4) into a relation between number of time-steps $(M+1)$ and number of x steps $(N+1)$, we assume, as in Endnote 5, that the limits of the x grid have been set so that

$$\Delta_x = \frac{2Q_x\sigma_x\sqrt{T}}{N+1},$$

where Q_x is a confidence multiplier (around 4) and σ_x some representative volatility of

the stock. Now (A.4) can be written

$$M+1 > (N+1)\frac{(1-\Theta)|\hat{r}_j - \hat{\gamma}_j|\sqrt{T}}{2Q_x\sigma_x} - \hat{r}_j T, \qquad j = 0, \ldots, M. \tag{A.5}$$

As, in most cases, the multiplier on $N+1$ is less than $0.05\sqrt{T}$, the constraint in (A.5) is not likely to interfere with the design of the finite difference mesh. We also point out, that (A.5) is only a sufficient condition; even if (A.5) is violated, the system (22) might be solvable. Indeed, in practice it appears to be very difficult to construct realistic examples where (22) cannot be solved.

Appendix B. Stability of the finite-difference scheme (21) or (22)

To simplify matters, let us assume that the interest rate in (21) is zero. A nonzero interest rate introduces some extra dampening of errors through discounting effects and will, if anything, lead to better stability properties than the case of zero interest rates. Now, equation (21) becomes

$$\begin{aligned} &H_{k-1,j}\left(-\tfrac{1}{2}\alpha(1-\Theta)(\hat{v}_{k,j} - \Delta_x\hat{b}_{k,j})\right) \\ &\qquad + H_{k,j}\left(1 + \alpha(1-\Theta)\hat{v}_{k,j}\right) + H_{k+1,j}\left(-\tfrac{1}{2}\alpha(1-\Theta)(\hat{v}_{k,j} + \Delta_x\hat{b}_{k,j})\right) \\ &= H_{k-1,j+1}\left(\tfrac{1}{2}\alpha\Theta(\hat{v}_{k,j} - \Delta_x\hat{b}_{k,j})\right) + H_{k,j+1}(1 - \alpha\Theta\hat{v}_{k,j}) + H_{k+1,j+1}\left(\tfrac{1}{2}\alpha\Theta(\hat{v}_{k,j} + \Delta_x\hat{b}_{k,j})\right) \end{aligned} \tag{B.1}$$

where $0 \leqslant \Theta \leqslant 1$ and $\hat{v}_{i,j} \geqslant 0$. We have used the suffix k instead of i as we will reserve i for the imaginary unit, $i = \sqrt{-1}$. To investigate the stability properties of the finite difference scheme, we consider a harmonic eigensolution of the form

$$H_{k,j} = \xi^{M+1-j}\mathrm{e}^{ik\omega\Delta_x}, \tag{B.2}$$

where ξ is the amplification factor (a complex number) and ω is the wave number (a real number). According to the Von Neumann criterion, stability of (21) requires that the *modulus of the amplification factor is less or equal to one*, independent of the wave number:

$$\forall\omega: \quad |\xi| \leqslant 1. \tag{B.3}$$

Inserting the eigensolution (B.2) into (B.1) and rearranging, we get

$$\xi = \frac{1 - \Theta\alpha\hat{v}_{k,j}(1-\cos\omega\Delta_x) + i\Theta\alpha\Delta_x\hat{b}_{k,j}\sin\omega\Delta_x}{1 + (1-\Theta)\alpha\hat{v}_{k,j}(1-\cos\omega\Delta_x) - i(1-\Theta)\alpha\Delta_x\hat{b}_{k,j}\sin\omega\Delta_x},$$

and hence

$$|\xi|^2 = \frac{\left(1 - \Theta\alpha\hat{v}_{k,j}(1-\cos\omega\Delta_x)\right)^2 + (\Theta\alpha\Delta_x\hat{b}_{k,j}\sin\omega\Delta_x)^2}{\left(1 + (1-\Theta)\alpha\hat{v}_{k,j}(1-\cos\omega\Delta_x)\right)^2 + \left((1-\Theta)\alpha\Delta_x\hat{b}_{k,j}\sin\omega\Delta_x\right)^2} \equiv \frac{U}{D}. \tag{B.4}$$

Both U and D in (B.4) are positive. To satisfy the stability criterion (B.3), we must

require that $D - U \geqslant 0$, or, after some manipulations,

$$\forall\omega: \quad 2\alpha\hat{v}_{k,j} + (1-2\Theta)\alpha^2\left[\hat{v}_{k,j}^2 + \hat{b}_{k,j}^2\Delta_x^2 + \cos\omega\Delta_x\left(\hat{b}_{k,j}^2\Delta_x^2 - \hat{v}_{k,j}^2\right)\right] \geqslant 0.$$

It follows that the finite-difference scheme (21) is stable if

$$0 \leqslant \Theta \leqslant \tfrac{1}{2}\left(1 + \frac{\dfrac{2}{\alpha}\hat{v}_{k,j}}{\hat{v}_{k,j}^2 + \hat{b}_{k,j}^2\Delta_x^2 + \left|\hat{b}_{k,j}^2\Delta_x^2 - \hat{v}_{k,j}^2\right|}\right), \qquad k = 1,\ldots,N, \quad j = 0,\ldots,M. \tag{B.5}$$

From (B.5) we conclude that the finite difference scheme is *unconditionally stable (that is, stable for all* $\hat{v}_{i,j} \geqslant 0$*)* if $0 \leqslant \Theta \leqslant \frac{1}{2}$. Both the fully implicit ($\Theta = 0$) and the Crank–Nicholson ($\Theta = \frac{1}{2}$) finite difference schemes are thus unconditionally stable. For the explicit scheme ($\Theta = 1$), however, stability is only guaranteed if, for all $k = 1,\ldots,N$, $j = 0,\ldots,M$,

$$\frac{2}{\alpha}\hat{v}_{k,j} \geqslant \hat{v}_{k,j}^2 + \hat{b}_{k,j}^2\Delta_x^2 + \left|\hat{b}_{k,j}^2\Delta_x^2 - \hat{v}_{k,j}^2\right|,$$

which is satisfied if

$$\hat{b}_{k,j}^2\Delta_t \leqslant \hat{v}_{k,j} \leqslant \frac{\Delta_x^2}{\Delta_t}. \tag{B.6}$$

In practice, the main problem is the upper bound, which puts a constraint on the spacing of the time grid

$$\Delta_t \leqslant \frac{\Delta_x^2}{\hat{v}_{\max}},$$

where $\hat{v}_{\max}$ is the largest local volatility in the mesh. As the required time spacing is a quadratic function of the x-spacing, the number of time-steps necessary to ensure stability will frequently be impractically high.

ENDNOTES

[1] The standard notation for volatility, σ, is reserved for instantaneous volatility; see equation (1).

[2] As we shall see in Section 4, there are probably circumstances where *no* choice of K and T will give the correct value. Some practitioners appear to overcome this problem by using two constant volatilities for knock-out options: one volatility determines the probability of breaching the barrier, and one volatility is used to price the terminal call option. Needless to say, such an approach does not make any theoretical sense.

[3] The approach taken by Rubinstein (1994) does not suffer from this problem. However, Rubinstein's method ignores the intertemporal nature of the volatility smile and only fits the terminal time-slice of the tree to the volatility smile. As such, the method is not suited for options where the payout is a function of the path of the stock price process (as is the case for American

and most exotic options). Recently, Jackwerth (1996) and Brown and Toft (1996) have developed methods to extend the Rubinstein approach to multiple option maturities. Both approaches are quite different from the one taken in this paper, though.

[4] This equation was independently derived by Andreasen (1996).

[5] For example, one could set

$$x_{N+1} = x_{\text{ini}} + \int_0^{\text{T}} [r(u) - \gamma(u)]\,\text{d}u - \tfrac{1}{2}\sigma_x^2 T + Q_x \sigma_x \sqrt{T},$$

$$x_0 = x_{\text{ini}} + \int_0^{\text{T}} [r(u) - \gamma(u)]\,\text{d}u - \tfrac{1}{2}\sigma_x^2 T - Q_x \sigma_x \sqrt{T},$$

where Q_x is a positive constant, x_{ini} is defined in (19), and σ_x is some representative constant volatility. If σ_x is properly chosen, setting Q_x to a value of, say, 4 will assure that the (risk-neutral) probability of the terminal stock price S_T falling outside the borders of the mesh is less than 0.01%.

[6] This assumption is not critical but simplifies the exposition. If the original stock price lies between nodes, various interpolation techniques can be applied.

[7] The 2nd-order convergence of the Crank–Nicholson scheme in Δ_t is due to the fact that its estimator of the time-derivative is *central* (as it is evaluated in the middle of t_j and t_{j+1}).

[8] The value of this contract does *not* equal the stock price S_{t_j} as the holder of the contract is not entitled to any dividends paid over the interval $[t_j, t_{j+1}]$.

[9] As a side-effect of the finite size of the finite-difference mesh, these prescribed values will not exactly equal the observable market prices. As a consequence, (32b, c) will sometimes lead to small spikes in the prices of Arrow–Debreu securities that pay out in the extreme upper and lower x boundaries of the mesh. This is no cause of concern as the absolute magnitude of these prices are typically $\ll 10^{-6}$ and hence have practically no influence on realistic option prices. At the price of a slight loss of accuracy, the spikes can be removed by abandoning (32b, c) and using the observable prices instead.

[10] The matrix Φ_j determines the scale of the quadratic program and only affects volatilities if the constraints are binding. In most cases, it is sufficient to set Φ_j equal to the identity matrix. For improved accuracy, particularly for long-term deals ($T > 5$ years), it is sometimes better to pick the call option payout matrix, $\{\varphi_{r,c}\} = \max(S_c - S_{r-1}, 0) = \max(\text{e}^{x_c} - \text{e}^{x_{r-1}}, 0)$, $r, c = 1, \ldots, N$. With this transformation, the quadratic program will optimize on option prices rather than Arrow–Debreu prices.

[11] Alternatively, one could interpolate directly on call option prices. Unless one is quite careful, this will tend to result in irregular implied volatilities, particularly for high and low strikes (where the sensitivity of option prices to implied volatility is low). Moreover, as noted in Andreasen (1996), it is easier to extrapolate and smooth on surfaces that are relatively flat (which presumably is the case for implied volatilities). Notice, however, that if stock forwards are themselves not smooth, as would for example be the case if dividends are modeled as discrete-time lump sum payments, it would not be appropriate to model implied volatilities (or call prices, for that matter) as smooth functions of T and K. Such cases can be handled by normalizing strikes with time-0 forward values

(F), i.e. we would write $\theta = \theta(K/F_T, T)$ and interpolate this function smoothly. Similarly, we would set $\sigma = \sigma(S_t/F_t, t)$ and modify the forward equation accordingly.

[12] While always yielding smooth Arrow–Debreu profiles, Shimko's method has a tendency to produce irregular local volatilities, particularly in the lower tail. Our experiments also show that the (nonlinear) search for tail distributions can be quite cumbersome.

[13] Here, we use the same mesh to price options with different strikes. The results can be improved slightly by adjusting the grid to ensure that each option strike coincides exactly with an x slice in the finite-difference mesh.

[14] The trade-off between smoothness and accuracy is similar to that of fitting yield curves to observed bond prices. If the objective is to generate a smooth forward curve, one must often rely on an approximate fit to bond prices (such as a regression spline).

[15] The Alpha 8400 5/300 is around 2 times faster than a 166 MHz Pentium II PC.

[16] While we use the Crank–Nicholson scheme in our example, we point out that this method can introduce spurious oscillations if the spot price is very close to the barrier. As Zvan *et al.* (1997) demonstrate, such oscillations can be eliminated by simply using the fully implicit method ($\Theta = 0$).

Volume 1/Number 2